Journal of Volcanology and Geothermal Research 259 (2013) 45–62

Contents lists available at SciVerse ScienceDirect

Journal of Volcanology and Geothermal Research

journal homepage: www.elsevier.com/locate/jvolgeores

Characterization of seismic events during the 2009 eruption of Redoubt Volcano, Alaska

Dane Ketner *, John Power

U.S. Geological Survey, Alaska Volcano Observatory, 4200 University Dr. Anchorage, Alaska 99508, United States

ARTICLE INFO

Article history:
Received 30 June 2011
Accepted 15 October 2012
Available online 24 October 2012

Keywords:
Redoubt
Volcano seismology
Multiplets
Swarms

ABSTRACT

Seismic events were automatically detected and characterized throughout the 2009 eruption of Redoubt Volcano, Alaska on a single short period station located 3 km from the volcanic crater. A total of 126,789 individual events were identified from continuous recording of seismic data from January 1 to June 30 (average 29 events per hour) using a short-term average/long-term average detection algorithm. Nine metrics were computed for this suite of events including event duration, inter-event time, event rate, peak amplitude, peak-to-peak amplitude, root-mean-square (RMS) amplitude, peak frequency, center frequency, and frequency index. Eight swarms were identified with event rates exceeding 100 events per hour. The first two occurred in late January and are attributed to high amplitude spasmodic tremor. Five additional swarms were manually repicked including swarms on February 26–27, March 20–23, March 27, March 29, and April 2–4. Three of these swarms immediately preceded major explosions including March 20–23, March 27, and April 2–4. A final swarm on May 2–9 was re-picked using a correlation detection scheme. We identified 146 event families that occurred within this suite of selected events using a cross correlation technique. Seven explosions were each immediately preceded by one or more event families. Events from the dominant family during each of these periods was additionally re-picked using correlation detection. The procession of event metrics and occurrence of event families formed a complex distribution throughout the eruption. A single-station approach was used to gain a fine-scale view of variations in seismic behavior at Redoubt with a focus on potential indicators of impending explosions. These techniques may serve an important role in future real-time eruption monitoring efforts.

Published by Elsevier B.V.

1. Introduction

Numerous studies of seismicity at active volcanoes have attempted to develop an understanding of active magmatic processes by associating the waveform character of individual seismic events with source processes. In these studies, seismic events are often classified based on their waveform appearance and the understanding of the causative or source processes. Several well developed classification systems for seismic events have been put forward in the past such as those by Minakami (1960), Latter (1979), Lahr et al. (1994). While successful, these studies have necessarily only classified a subset of the thousands of seismic events that may have occurred during an eruptive episode at an individual volcano. Moreover, they have frequently been limited to events that were large enough to record on numerous seismic stations allowing for hypocenter and magnitude calculations. As a result, information from small events that may only record on the station or stations closest to the volcanic vent may be missed resulting in an incomplete chronology of the progression of seismic events throughout the course of eruptive activity.

In this study, we developed a more complete characterization of the progression of seismicity associated with the 2009 eruption of Redoubt Volcano. This analysis covers six months of data from January 1 through June 30, 2009 (all times in UTC). Secondly, we evaluated automated procedures for detecting and characterizing volcano seismic events which may prove useful in tracking future seismic unrest at Redoubt and other similar volcanoes. We used a short-time average/long-time average (STA/LTA) (Allen, 1978) event detector to identify seismic events on a single seismic station, REF, located 3 km from the volcanic crater. Once events were identified, we calculated the event duration, inter-event time, event rate, peak amplitude, peak-to-peak amplitude, root-mean-square (RMS) amplitude, peak frequency, center frequency, and frequency index (Buurman and West, 2010). This approach was motivated by recent investigations that have developed automated event classifications at Mount St. Helens (Moran et al., 2008; Qamar et al., 2008) and Augustine Volcano (Buurman and West, 2010). In addition, we also use waveform cross correlation techniques to identify the occurrence and progression of families of repeating earthquakes or multiplets throughout the 2009 eruption sequence.

This analysis revealed eight swarms, or time periods when the seismic event rate was anomalously high. For five of these swarms, we manually repicked events thereby guaranteeing a near complete record of all

* Corresponding author.
E-mail address: dketner@usgs.gov (D. Ketner).

0377-0273/$ – see front matter. Published by Elsevier B.V.
http://dx.doi.org/10.1016/j.jvolgeores.2012.10.007

events occurring during these periods while also ensuring that false events generated by noise were removed. Between May 2 and 9, the rate of seismic events was so high that the manual procedure was untenable. Events during this period were repicked using an evolving correlation detection scheme similar to Stephens and Chouet (2001). This same scheme was also used to detect seven multiplets that were precursory to explosions between March 23 and April 4.

We begin this paper with a short description of the 2009 eruption of Redoubt Volcano and the instrumentation available to track seismicity during the study period. We then describe the methodology used in single-station detection (SSD) as well as the automated metrics used to classify events and remove noise. We use the characterization of individual events to develop a detailed chronology of seismic event character throughout the 2009 Redoubt eruptive sequence. This is followed with a discussion of some of the major trends from the eruption sequence. We conclude with an evaluation of the various automated metrics used to characterize seismic events and recommendations for future analysis of Redoubt seismicity. Details of the STA/LTA event detection algorithm and the procedures for detecting noise are summarized in Appendix A and B respectively.

2. Redoubt Volcano

Redoubt Volcano is an active stratovolcano located 170 km southwest of Anchorage, Alaska (see Bull and Buurman (2013) for additional details about the location and eruptive history of Redoubt Volcano). Redoubt has erupted at least five times since 1900 including 1902, 1933, 1966–68, 1989–90 and 2009. The 2009 eruption was the second eruption to be monitored seismically. The 1989–90 and 2009 eruptions were characterized by explosive events that are often separated by the quieter effusion of lava that forms domes within the summit crater (Power et al., 1994, 2013). Specific hazards associated with eruptions at Redoubt include lahars which threaten the nearby Drift River Oil Terminal, and especially ash plumes which threaten the busy airspace around Anchorage International Airport. The 1989–90 explosions generated 23 ash plumes reaching heights 8–12 km above mean sea level (ASL) (Miller and Chouet, 1994) while the 2009 eruption had 20 explosions with at least 16 sending ash columns to heights of 8–18 km (ASL) (Bull and Buurman, 2013).

2.1. Seismic network

The telemetered Redoubt subnetwork consisted of six Mark Products L4 single-component short-period instruments, two Mark Products (L4 and L22) three-component short-period instruments, and two Guralp CMG-6TD three-component broadband instruments. The two broadband stations (RDWB and RDJH) were installed in 2009 after unrest began. Four temporary campaign broadband stations (RDW, RD01, RD02, and RD03) were placed on the volcano to capture the 2009 eruption. These stations stored data internally and were not available for real-time analysis. Table 1 lists all stations recording within the Redoubt subnet during the eruption. Locations of all Redoubt seismic stations are shown in Fig. 1. Periods of station operation are shown in Fig. 2. Note that 'operational' signifies that the station was transmitting data and does not imply that usable seismic data was produced. RED is probably the most significant example of this as all data is heavily overlain with electronic noise.

2.2. AVO analyst-reviewed catalog

AVO maintains an analyst-reviewed catalog (*ARC*) of located earthquakes at volcanoes with seismic instruments. The 2009 ARC included 4246 earthquakes within the Redoubt subnetwork (Dixon et al., 2010). Phase arrivals for triggered events are interactively picked using XPick (Robinson, 1992) and located with Hypoellipse (Lahr, 1999) on a daily basis. To be located, events have to display a minimum of three P-phases and two S-phases with standard hypocentral errors less than15 km. Events that do not meet this criteria are discarded. The result is a smaller high-quality catalog of locatable events with a VT-bias as a result of the S-phase requirements. Catalog events are used in this study to supplement our single station detections.

Table 1
Seismic instrument station short-hand names are shown in the first column, along with date of installation, specific type of seismometer instrument, and the number and type of channel components. 'BH' indicates the station was a digital broadband instrument, all of which had three components: vertical, north, and east. 'EH' indicates the station was a short-period analog station, all of which contained a single vertical component with the exception of REF which contained a vertical, north, and east component.

Station	Installed	Seismometer	Comp
DFR	8/15/1988	L-4	EH1
NCT	8/14/1988	L-4	EH1
RD01[a]	3/21/2009	CMG-6TD	BH3
RD02[a]	3/20/2009	CMG-6TD	BH3
RD03[a]	3/20/2009	CMG-6TD	BH3
RDE	2/4/2009	L-4	EH1
RDJH	2/4/2009	CMG-6TD	BH3
RDN	8/13/1988	L-4	EH1
RDT	8/9/1971	L-4	EH1
RDW[a]	3/21/2009	CMG-6TD	BH3
RDWB	2/4/2009	CMG-6TD	BH3
RED	8/30/1990	L-4	EH1
REF	7/27/1992	L-22	EH3
RSO	3/1/1990	L-4	EH1

[a] Campaign stations (not telemetered).

2.3. 2009 eruption

The 2009 eruption is characterized by the formation of a sequence of lava domes in the summit crater and a sequence of 20 explosive events (labeled numerically, 0–19, by Schaefer (2012)) that occurred between March 15 and April 4, 2009. The 2009 eruption sequence is typically described as consisting of a precursory, explosive, and continuous phase with transitions at the first and last magmatic explosions (1 and 19) on March 23 and April 4 respectively. Effusion of the final lava dome ended on July 15 (Diefenbach et al., 2013). All dates and times referred to throughout the remainder of this study are UTC.

2.3.1. Precursory phase (November 2008–March 23, 2009)

Gas emissions and increased melting of the summit glacier ice were the first signs of unrest at Redoubt prompting AVO to raise the volcano alert level and aviation color code to 'Advisory'/Yellow on November 5, 2008. A complete timeline of color code and alert level changes can be

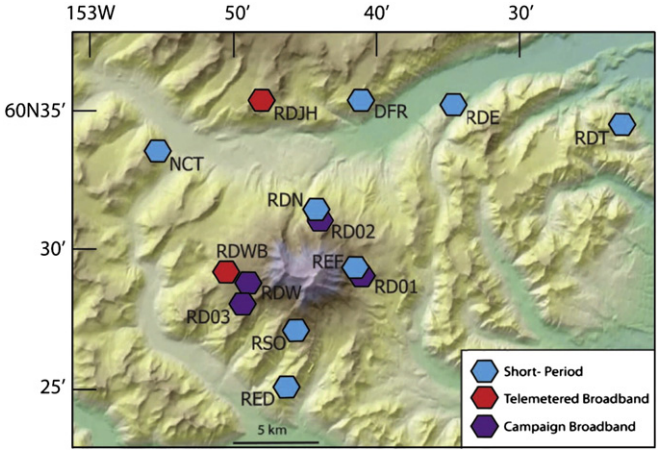

Fig. 1. Map showing locations of seismic stations that operated near Redoubt Volcano in 2009.

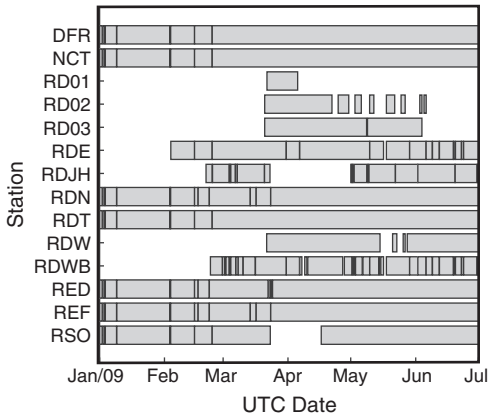

Fig. 2. Solid horizontal bars indicate time periods when individual seismic stations in the Redoubt network were operational. Station outages of less than 1 h are not shown.

seen in Table 1 of Schaefer (2012). Deep LP events at depths 25 to 38 km below sea level began to occur in December of 2008 (Power et al., 2013). Geodetic data provides supporting evidence that an intrusion of magma may have occurred at these depths (Grapenthin et al., 2013). Seismicity remained near background levels in early January 2009 until 5 h of energetic tremor was observed on January 25 prompting AVO to raise the alert level and color code to 'Watch'/Orange. These initial tremor episodes were followed by a complex seismic sequence containing periods of volcanic tremor, individual events, and periods of quiescence until March 22. The character of this period of seismicity is described by Buurman and West (2013) and Power et al. (2013). Summary helicorder plots and an RSAM record from station RSO (Fig. 1) are shown in Fig. 6 of Power et al. (2013). AVO dropped the alert level and color code to Yellow on March 10 after a prolonged period of quiescence. A small phreatic explosion (event 0) lead to a color code elevation (Orange) on March 15 which was again lowered to yellow on March 18. An intense swarm of shallow events began on March 20 prompting AVO to return once again to Orange on March 22. This swarm culminated in the first magmatic explosions on March 23, 2009.

2.3.2. Explosive phase (March 23–April 4, 2009)

A swarm of shallow events containing numerous families began roughly at 12:00 on March 20 at depths 3–6 km below the crater floor (Power et al., 2013), and intensified in amplitude and rate until turning into strong tremor in the last hours leading to an explosion on March 23 at 06:38 (explosion 1). A small newly extruded dome was visible in satellite imagery on March 22, prior to the explosion. Analysis in this study found the swarm to be uniquely heterogeneous compared to all other precursory swarms from 2009. A total of 28 separate families were detected which ranged greatly in size and spectral content.

Four more explosive events occurred within 6 h (explosions 2–5), the last on March 23 at 12:31. Another explosion occurred on March 24 at 3:41 (explosion 6) which was preceded by over 200 lower amplitude multiplet events. Seismic levels subsided until two explosions occurred on March 26 at 16:34 and 17:24 (explosions 7 and 8). A strong swarm began early on March 27 which increased in amplitude for about 8 h and clipped the summit stations. Calculated local magnitudes for these events ranged from 0.4 to 1.8 (Dixon et al., 2010). Events merged into continuous tremor approximately 8 min prior to an explosion at 7:47 followed by another at 8:28 (explosions 9 and 10). These mark the first two instances of gliding harmonic tremor prior to explosions (Hotovec et al., 2013). There is insufficient data to confirm whether or not a dome had extruded prior to these explosions. Eight more explosions occurred between 16:39 on March 27 and 3:23 on March 29 (explosions 11–18). Of these, explosions 12 and 18 were directly preceded by multiplets. A multiplet swarm began on March 29 at 07:50 which lasted 70 min but did not end with an explosion. An increase in the rate of large low-frequency events began after explosion 18 which lasted through the remainder of the explosive phase and well into the continuous phase. Observations of a second confirmed dome were made on March 29, which grew considerably in volume throughout the remainder of the explosive period. On April 2 at 19:00, a swarm of emergent, low amplitude, low frequency events began which lasted for nearly 48 h and culminated in the final and most energetic explosion of the 2009 sequence on April 4, at 13:59 (explosion 19). Hours prior to this explosion, VT earthquakes began to occur which continued throughout the remainder of the study period.

2.3.3. Continuous phase (April 4–July 15, 2009)

This period is characterized by growth of a single dome which began immediately following the April 4 explosion and continued until mid July. An increase in the number of high frequency brittle failure events, many of which formed families, occurred throughout this period at depths 3 to 9 km below the crater floor, consistent with the suggested magma source region (Power et al., 1994, 2013). A pattern of increased large low frequency events continued after explosion 18 through April and early May. A final decline in these events coincided with the appearance of a swarm of emergent, low amplitude, low frequency events on May 2–9 which group nearly exclusively into a single family. The number of events detected from this family far exceeded that of all other multiplets combined during the 2009 eruption sequence. This swarm is temporally consistent with observations of changes in dome extrusion behavior and rate (Bull et al., 2013), changes in dome chemical composition (Coombs et al., 2013), and increased gas emissions (Lopez et al., 2013). On May 6, an hour-long series of rockfalls from the dome was recorded followed immediately by a dramatic change in the procession of the swarm events. By the end of May9, the swarm had ended. A steady succession of both low and high frequency events continued throughout May and June, though at a greatly reduced rate.

3. Methodology

3.1. Event detection and metrics

Single-station detection (SSD) was performed from January 1 to June 30, 2009 on vertical channel data using a basic short-term average/long-term average (STA/LTA) algorithm, details of which are provided in Appendix A. The station REF was identified as the best candidate for use as a master station in SSD due to its consistent operation (Fig. 2), proximity to the summit crater, and good signal-to-noise ratio (SNR).

Once events were identified, nine metrics were used in differing capacities throughout this study to characterize individual seismic events including three temporal, three amplitude, and three spectral metrics. Some metrics like RMS amplitude and frequency index (FI) were used to characterize seismic events consistently throughout the 2009 eruption. Other metrics like peak-to-peak amplitude and center frequency were used only to identify outlier noise and low-SNR events. We note that amplitude measurements were not instrument corrected since amplitudes were not directly compared between stations. Seven of the nine metrics produce a single value per event including duration, peak amplitude, peak-to-peak amplitude, RMS amplitude, peak frequency, center frequency, and frequency index. The remaining two metrics include interevent time which produces one less value than number of events, and event rate which produces a number of values proportional to time lapsed. The metrics used include:

(1) Duration — The length in seconds of the event as determined by the distance between the SSD trigger on and trigger off times (Appendix A). In general, larger events have longer durations.
(2) Interevent time — Also called 'interevent spacing', this metric determines the amount of time elapsed between consecutive

event triggers. Any array of N events will therefore have N-1 interevent time values.

(3) Event rate — Event rate is the time averaged inverse of interevent time. Throughout this study, event rate is computed on an hourly basis by counting the number of events that begin within hour long blocks.

(4) Peak amplitude — This value is determined from the highest absolute value of demeaned event waveform data. This metric is useful in determining when a station is clipping.

(5) Peak-to-peak amplitude — Similar to peak amplitude, this is a simple subtraction of the lowest point from the highest point of the event waveform. When used with peak amplitude, this metric performs well as a noise detector.

(6) Root-mean-square (RMS) amplitude — RMS amplitude is computed over a 5.12 s window which is centered to maximize the value for each event. This provides a good relative measure of the amount of seismic energy observed at a single station and is also useful for determining variation in event size above the clipping threshold.

(7) Peak frequency — This metric measures the single highest real frequency as determined by Fourier analysis. A 1024 point FFT was computed over a 5.12 second window centered on the highest average amplitude portion of the demeaned event waveform. The resulting real frequency values were separated by 0.0976 Hz ($\frac{F_{NYQUIST}}{512}$). A cosine tapered was finally applied to the first 10 real FFT values to avoid spurious peaks near 0 Hz.

(8) Center frequency — Center frequency is the frequency value which minimizes the difference between the sum of all spectral amplitudes above and below that value computed between 0 Hz and the Nyquist frequency at 50 Hz. The FFT is computed in an identical fashion to peak frequency over the highest average amplitude 5.12 second window.

(9) Frequency index (FI) — This is a spectral ratio defined as $FI = log_{10}\left(\frac{mean(A_{upper})}{mean(A_{lower})}\right)$, which was designed to provide a consistent classification of seismic events (Buurman and West, 2010). This method uses the mean amplitude of two spectral bands (A_{upper} and A_{lower}) to describe the relative spectral content of a single event. Buurman and West (2010) used 10 to 20 Hz for A_{upper}, and 1 to 2 Hz for A_{lower} and found low FI values to be a good indicator of impending eruption at Augustine Volcano in 2006. Initial analysis showed that a majority of spectral energy was occurring between 2 Hz and 10 Hz at Redoubt, and thus the spectral bands were extended to 8 to 25 Hz for A_{upper}, and 2 to 4 Hz for A_{lower}. This study performs FI analysis over the highest average amplitude 5.12 second window of an event waveform with the same FFT parameters as the peak frequency metric. This differs from the 7 second window beginning one second before the earthquake triggers used by Buurman and West (2010). This alteration was made to adapt to the presence of many low amplitude events.

3.2. Noise detection

Visual examination of helicorder records displayed periods of abundant electronic noise existing throughout portions of the continuous data. Electronic noise was removed from the waveform data of station REF:EHZ by omitting about 1342 periods of noise-compromised data and instrument calibration pulses identified by manual examination of both seismograms and spectrograms. The cumulative amount of removed data totaled 1.63 days of data or 0.9% of the study period. Over 75% of this noise occurred between April 14 and April 20. Fortunately this time period did not contain any large volcanic events (Bull and Buurman, 2013).

Severe periods of noise contamination including those with greater duration and amplitude were all identified manually. Despite this effort, many noise-related events continued to be detected. This motivated an approach whereby events would be detected automatically as real or noise-related using event metrics. By exploring the upper and lower extreme ranges of these values, we were able to identify particular metrics and ratios between multiple metrics which were generated almost exclusively by electronic noise or low SNR events. The singular metrics and metric ratios used in noise detection include: RMS amplitude, peak frequency, center frequency/peak frequency, peak-to-peak amplitude/RMS amplitude, and frequency index. The threshold values for noise determination are summarized in Appendix B. To determine these thresholds, clusters of 40 events were selected immediately above or below a given threshold and tallied as either noise or non-noise events. The threshold was adjusted until 50% of events in a group were noise events. In addition to manually removed sections of waveform data, a total of 9881 noise events were stripped using the developed automatic procedure. This represented 7.2% of the original 136,670 events resulting in a final set of 126,789 SSD events.

3.3. Swarm analysis

The SSD hourly event rate was used to identify periods of swarm activity. Eight periods when the SSD hourly event rate exceeded 100 events per hour were identified between January and July 2009. For discussion, we refer to these individual swarms as 'T' for tremor swarm (these occurred during precursory phase tremor), 'P' for precursory swarm (These immediately preceded explosive events), or 'S' for any swarm that is not a T or P swarm. The swarms occurred in this order: T1 (Jan 25), T2 (Jan 30–31), S1 (Feb 16–17), P1 (Mar 20–23), P2 (Mar 27), S2 (Mar 29), P3 (Apr 2–4), and S3 (May 2–9). Beginning and ending times for all swarms were determined manually based upon an examination of helicorder records, except for S3, which was determined via a correlation detection algorithm (Section 3.5). Swarm start and stop times used by this study are summarized in Table 3.

To provide a more complete characterization of seismic events within swarms S1, P1, P2, S2, and P3, individual events were manually re-picked by scrolling through dual seismogram/spectrogram displays of continuous data from REF:EHZ. A customized computer application allowed for rapid event selection while viewing data in both time and frequency domains. This system generated spectrograms containing second long bins of spectral values between 0 Hz and 25 Hz. Though a single-station bias still existed for these picks, the resulting event set proved to be more complete and accurate than that generated from SSD which relied solely on the STA/LTA algorithm (Appendix A). This process was performed to gain a high resolution set of seismic events from the swarms and would have been an overwhelming process to perform throughout the entire eruption. The S3 swarm on May 2–9 was the single exception which was not manually re-picked due the sheer quantity of events present which was greater than all previous swarms combined. A detailed description of the correlation detection scheme is given in Section 3.5.

3.4. Multiplet identification

To identify earthquake multiplets (families of events with similar waveforms) from the series of SSD events, and also from manually picked events, we used a cross-correlation technique with a hierarchical clustering scheme. To be successfully clustered into a family, an event must have a minimum mean correlation value of $CC = 0.75$ with all other events in the family. This scheme was successfully employed to detect multiplets at Augustine Volcano (Buurman and West, 2010). We changed the 7 second cross-correlation window used previously at Augustine to a 6 second window to better fit the set of SSD events which had a mean duration of 6.2 s. A shorter correlation window length ensured that smaller amplitude repeating events would successfully form families. This also increased the possibility of correlated noise signals clustering into families. To account for this, waveforms from each family were manually inspected and

those that had obvious noise signals were discarded. Because of the great wealth of multiplet activity at Redoubt, a minimum threshold of 10 events was used to keep the total number of studied families to a manageable size.

The computer memory available during this research put certain limitations on the size of cross-correlation matrices that could be computed at once. The set of SSD events, as well as the manually picked event series from the P1 and P3 swarms were too large to compute en masse given our computer resources. To overcome this, an iterative cross-correlation method was used on subsets of 2000 events. In this method, each subset overlapped the previous subset by 1000 events, thereby allowing arrays of family member references to be passed from subset to subset. This also implied that a family would expire if members are distributed in time by greater than 2000 events which represented a theoretical short-coming of this method.

Finally, dominant families that were precursory to explosions as detected by SSD cross-correlation were also repicked using a correlation detector described in Section 3.5. These precursory multiplets were detected prior to explosions 1, 3, 6, 9, 12, 18, and 19 which includes all three precursory swarms. Correlation detection identified many multiplet events that had been missed by SSD offering an even more complete picture of event procession prior to explosions. Results from multiplet detection for both manually-picked swarm events, and SSD events are examined in detail in Section 4.2 and Section 4.3. All seven multiplet clusters which preceded explosions are examined in Section 4.4.

3.5. Correlation detection

Events from certain families of interest were detected using an adaptive correlation detection scheme similar to that used by Stephens and Chouet (2001) to detect LP events throughout the 1989 precursory swarm at Redoubt. A similar technique was used by Haney et al. (2009) to track repeating explosions at Pavlof during the 2007 eruption. This automated technique proved robust at detecting events from a single family, even when individual events were low in amplitude. Correlation detection was used to detect events from the dominant families which preceded explosions 1, 3, 6, 9, 12, 18, and 19. Correlation detection was also used to detect events from the S3 swarm which contained far too many events to be re-picked manually.

In this technique, a single reference event was initially selected from each family which had high SNR and correlated well to other events within their family. A six second window of the highest amplitude portion of each waveform was then isolated. These waveforms were incrementally correlated against continuous data from REF: EHZ both forwards and backwards through time starting from the time of each original reference waveform. Correlation values above the threshold value ($CC = 0.7$) were tracked. If multiple consecutive values existed above the threshold, then only the maximum value was recorded. The time of each correlation peak was then recorded, and a superposition of the newly detected six second waveform scaled by .1, and the existing reference waveform scaled by .9 became the new reference waveform. This weighted superposition of the existing reference waveform with newly detected waveforms allowed the reference to quickly adapt to waveform changes that might occur over time due to any alteration in the source or path. If two events were detected within less than 3 s of each other, the event with the greater *CC* value was recorded, and the other was discarded. The use of a 3 second minimum event spacing ensured that a single event wouldn't be recorded multiple times, and that events wouldn't be lost from this detection as event spacing became very small as they did during the S3 swarm.

Our 6 second window was significantly shorter than the 10 second window used by Stephens and Chouet (2001). This reduced window length was chosen to adapt this technique to the events with reduced amplitude and duration as found in the P3 and S3swarms. Our correlation threshold for the detector ($CC = 0.7$) was also set higher than that used previously ($CC = 0.68$) to account for our reduced window size. Variation in threshold values between 0.65 and 0.75 primarily affected the number of low SNR events that were detected without substantial addition or loss of events overall. The correlation value we chose represented a balance between the number of events detected, and an acceptable SNR level. The algorithm was run continuously forwards and backwards though time until events became separated by 1.5 h or more. Initial tests of this threshold found that even at 8 h, very few outlier events were being detected.

4. Results

4.1. Single station detection

SSD events assumed a wide range of temporal, spectral, and amplitude values with a complex distribution throughout the study period. Selected metrics from the 126,789 individual events are summarized in Fig. 3. Maximum, minimum, mean, and median values for event spacing, duration, peak amplitude, peak-to-peak amplitude, RMS amplitude, peak frequency, center frequency, and frequency index (FI) were computed over the precursory, explosive, and continuous phases of the eruption as well as the eight identified swarms and are displayed in Fig. 4. Fig. 5 contains a summary of the rate and FI of larger events as well as example waveforms. A summary of very broad observations from SSD metrics includes:

(1) Eight periods met or exceeded the 100 events/hour threshold and were declared swarms. These ranged in duration from a week to just over an hour. Amplitude and frequency values varied greatly between swarms and also within swarms. The P1 swarm displayed a much greater range of values and evolution through time while others like the P3 and S1 swarm were more homogeneous. A peak of 98 events/hour occurred on March 24 but was not classified as a swarm as the event rate did not meet the threshold set in this study (Fig. 3A)
(2) High event amplitudes formed distinct clusters between the T1 and S1 swarms (Jan 25 to Feb 26), between the P1 swarm and explosion 6 (Mar 20 to 24), and between the P2 swarm and the end of March (Mar 27 to 31).
(3) High frequency events were present throughout the eruption with one notable period of quiescence between the T2 and S1 swarms. The single largest increase in the rate of high frequency events occurred before the first magmatic explosion on March23. A greater concentration of high frequency events occurred throughout the continuous phase with the period late April and early May being the most pronounced (Figs. 3, 4, 5).
(4) Very low frequency events (FI < −1.4) began in late January consistent with swarms T1 and T2. Events had low spectral content, low events rates, and high amplitudes throughout much of February. A dramatic increase in the rate of larger low frequency events began following the second to last magmatic explosion on March 29. These events continued at an unprecedented rate throughout April (Figs. 3G, 5B).

Overall, SSD performed well in its capacity to identify and characterize events and document even subtle variations in seismicity throughout the study period. Inherent in each metric were strengths and weaknesses that we have summarized in Table 2. Analysis of event metric values leading up to magmatic explosions revealed that no single obvious trend within the suite of metrics and analysis performed here could accurately predict impending explosions without also falsely identifying periods that did not result in explosion. Regardless, event rate – which remains one of the of the most fundamental metrics – did successfully indicate explosive conditions during all three major precursory swarms.

Frequency index was the most useful metric for visualizing spectral trends throughout the eruption. One difficulty with this metric however, was the effect of low SNR. Events with lower amplitudes tended to have higher FI values resulting from higher frequency background noise

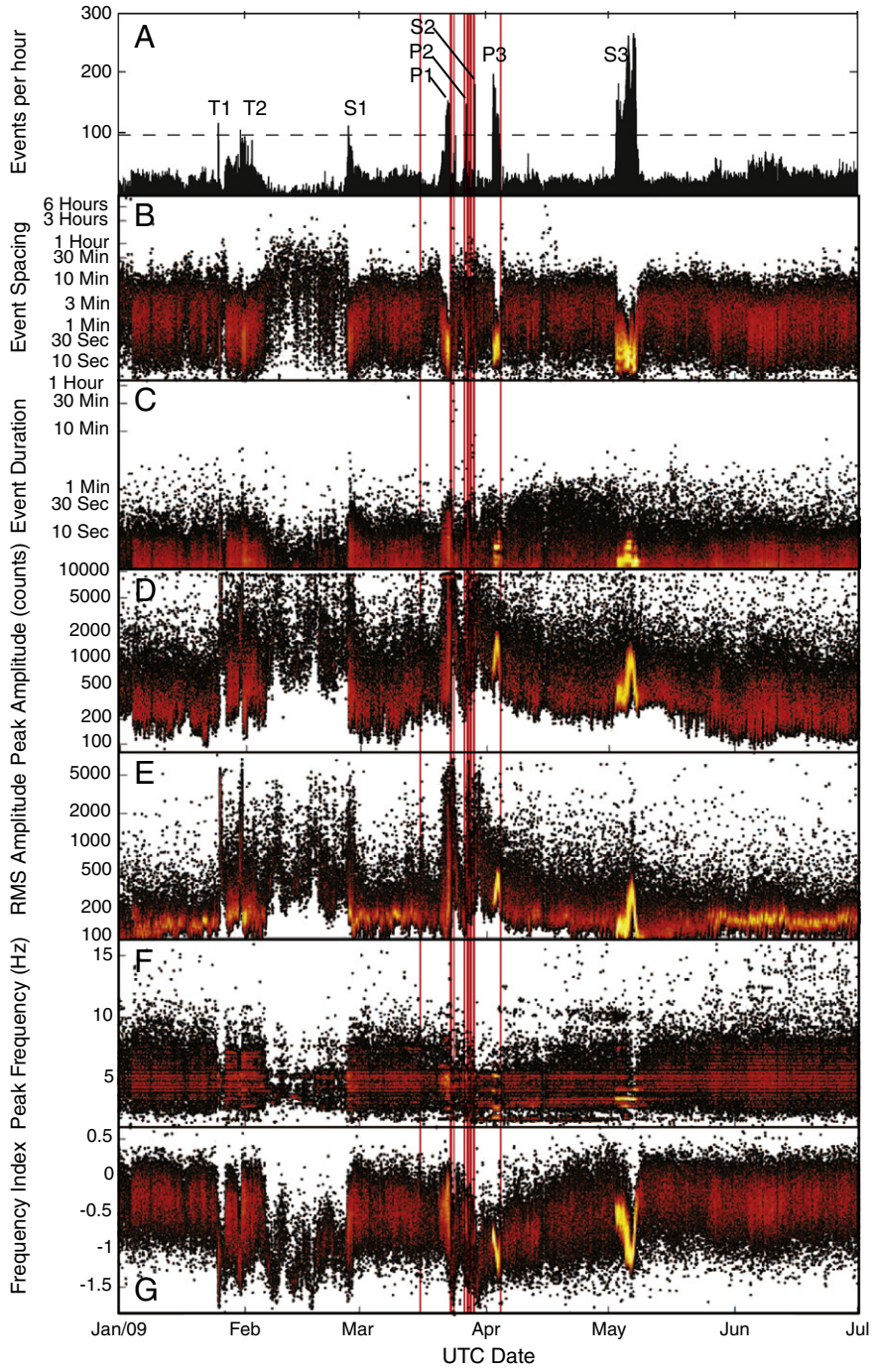

Fig. 3. Metrics from 126,789 SSD events from January 1 to June 30, 3009 from top to bottom: (A) hourly event rate, (B) event spacing, (C) event duration, (D) peak amplitude, (E) RMS amplitude, (F) peak frequency, and (G) frequency index. Explosions 0–19 are shown as red vertical lines. Saturated portions of each scatter plot have been overlayed with a shaded color image indicating relative point density. black-red-orange-yellow-white indicates increasing density of points in the scatterplot.

contributing more to the overall event spectra. This inverse relationship between FI and amplitude values was most pronounced at RMS amplitude values of 250 or less. To observe overall spectral trends not skewed by low SNR, a subset of 11,297 'large' events were selected from the SSD set. This set included events with RMS amplitudes greater than 250 and durations longer than 8 s. Fig. 5 charts the progression of these larger events throughout the eruption which were split into 6 subsets of higher and lower FI values based on an adjusted mean and standard deviation. The cumulative event count from these six event groups helped to illuminate where higher and lower frequency events were occurring throughout the eruption. The P1 swarm for instance showed large gains in medium to high frequency events, though a consistent accumulation of very high frequency events didn't begin until mid-April.

Of the 126,789 SSD events, only 2% (2684 events) were located by AVO from the Redoubt subnetwork (Dixon et al., 2010). Fig. 6 displays earthquake spectral amplitude (ESAM) (Moran et al., 2008) for all located events and earthquake focal depth vs. time. In this plot, earthquake hypocentral depth is referenced to sea level and negative values reflect height above sea level. The clustered line of events at −3 km are events that located at the top of the 1-dimensional velocity model used in event location. The clustering of these shallow events is an artifact of both varying hypocentral error, and the constraint that events

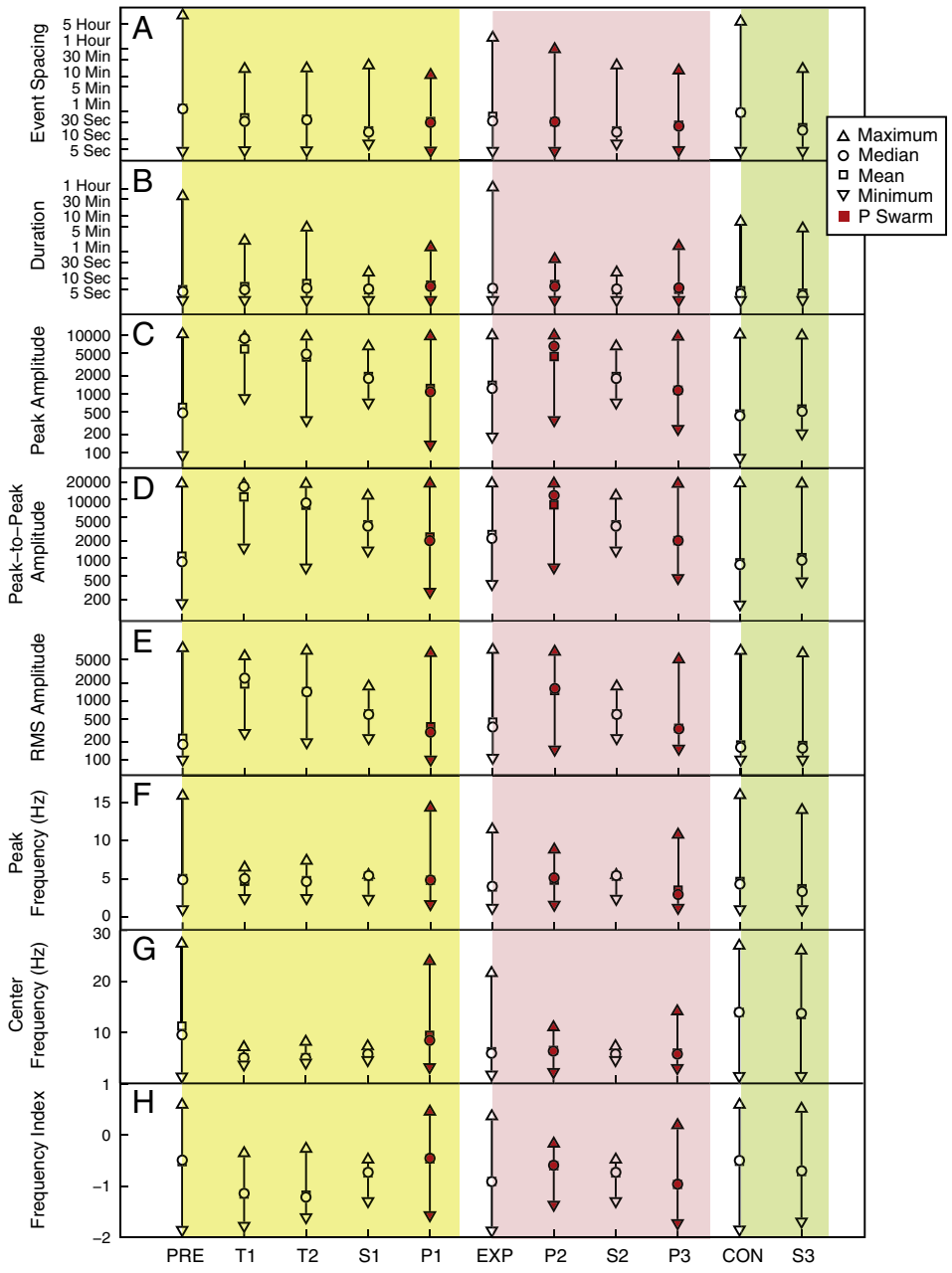

Fig. 4. Statistical values are displayed for (A) event spacing, (B) duration, (C) peak amplitude, (D) peak-to-peak amplitude, (E) RMS amplitude, (F) peak frequency, (G) center frequency, and (H) frequency index during each phase of the eruption, as well as for individual swarms. The swarms over which values are computed are listed on the x-axis. The times of each swarm are listed in Table 3. 'PRE','EXP', and 'CON' indicate that values were calculated over the entire precursory, explosive, and continuous phases. Values derived from swarms that preceded explosions (P1, P2, and P3) are highlighted in red.

cannot occur higher than the volcanoes summit (Power et al., 2013). Shallow events are present throughout the precursory phase with a distribution of deeper events extending from depths of 0 to 10 km BSL. The P1 swarm (March 20–23) follows this trend, though most deeper activity is constrained to depths of 0 to −3 km. Events from swarm P2 (March 27) are larger in magnitude than P1 and locate almost exclusively above 1 km. The two longest swarms of 2009 (P3 and S3) occurring on April 2–4 and May 2–9 are largely missing from this catalog due to low event magnitudes. Most of these events did not meet the minimum number of phase arrivals required for hypocentral location (Dixon et al., 2010). Many deeper high frequency events occurred beginning in April including one magnitude 3.5 earthquake on April 9 which is the largest magnitude earthquake ever located at Redoubt (Power et al., 2013). These VT events located deeper than lower frequency events with few approaching the −3 km ceiling. April likewise contained many shallow lower frequency events accounting for a great majority of events at and above sea level. Shallow ARC events largely disappear by the end of April while higher frequency events at depths 0 to 8 km persist throughout much of May.

4.2. Swarms

The eight swarms detected via SSD hourly event rate are listed in Table 3 including start and end times, maximum event rate, and cumulative event count from both SSD and manually repicked events. Values for event spacing, peak amplitude, RMS amplitude, peak frequency, and frequency index from all manually re-picked swarms are

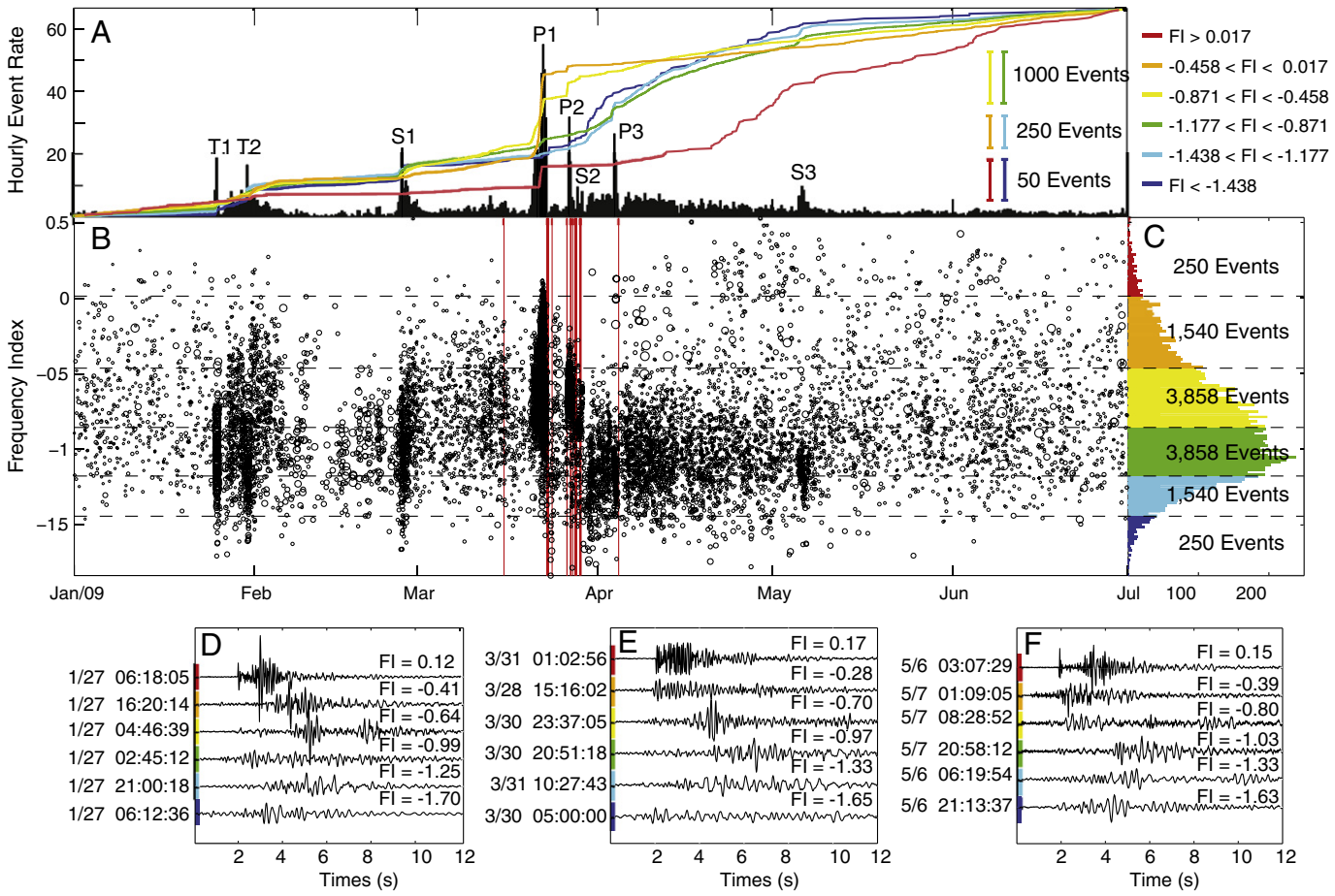

Fig. 5. The procession of a subset of 11,297 'large' SSD events (RMS amplitude values greater than 250, and durations greater than 8 s) are summarized including (A) hourly event rate (black bars) and cumulative event count for events grouped by frequency index values (colored lines). Events were divided into 6 color-coded groups based on an adjusted mean and standard deviation of FI values such that events were evenly divided at both extremes. Red events had the highest FI values ($FI > 0.017$) while blue events had the lowest FI values ($_{cx}$). Scaling of cumulative event count (colored lines) on the vertical axis depended on the number of events in each group. (B) Event FI values are plotted with marker size proportional to RMS amplitude and vertical red lines indicating times of explosions 0–19. (C) The total number of events in each group is listed over the corresponding portions of an occurrence histogram. The histogram is split into 100 increments on the vertical axis corresponding to FI values 0.55 through −1.85 with an approximate width of 0.015. The number of events within each increment is displayed along the horizontal axis. (D, E, F) Example waveforms from each group are displayed from the precursory, explosive, and continuous phases as well as their computed FI values.

displayed in Fig. 7. These swarms are examined in chronological order in the remainder of this section.

4.2.1. T1,T2 swarms (January 25, 30–31)

On January 25 and 30, event rates from SSD peaked at 119 and 108 events per hour respectively during periods of intense spasmodic tremor. At REF, the tremor amplitude was highly spasmodic leading to the high event detection rate at this station, but the tremor 'events' themselves lacked the broad spectral onsets and transition to lower frequency that is often associated with discrete low frequency events at Redoubt (Chouet et al., 1994). Individual events were not re-picked manually due to the ambiguity of identifying start and stop times amid the persistent overlying tremor. Instead, frequency and RMS amplitude were computed over continuous minute-long sections of each swarm displayed in Fig. 8.

4.2.2. S1 swarm (February 26–27)

The first manually repicked swarm examined by this study began after a 1.5 hour burst of high amplitude tremor early on February 26. The swarm contained 1631 events that were manually selected from REF:EHZ between 3:00 February 26 and 13:00 February 27. Most of these events had smaller amplitudes and durations (Fig. 7), while 60 of these events (nearly 4%) had amplitudes sufficient to clip station REF. Many of these large events had emergent onsets with unclear phases, or waveforms that appeared to contain multiple overlapping events resulting in exclusion from the analyst catalog as a result of large hypocentral errors. This swarm contained the largest amplitude events of any swarm, some of which had waveforms similar to events earlier described as explosions at Redoubt by Power et al. (1994).

Waveforms from this swarm generally correlated poorly with less than 8% forming multiplets of 10 or more at station REF. Two clusters of multiplets occurred between 6:00 and 15:00 on February 26, and between 5:00 and 13:00 on February 27. The first cluster contained three families of 16, 45, and 28 events while the second contained one family of 37 events. Each family had one or two stable spectral peaks ranging from 5.6 Hz to 4.1 Hz, though these peaks were dissimilar between families (Fig. 7D).

4.2.3. P1 swarm (March 20–23)

The P1 swarm began at 12:00 March 20 and contained 4900 manually picked events. Event metrics are displayed in Fig. 7. Event rate was low initially, but steadily increased to a maximum of 209 events per hour at 17:00 March 22. Event rate declined rapidly after a final peak of 173 events per hour occurred at 3:00 March 23. Individual events became difficult to discern as overall amplitudes increased steadily becoming continuous high amplitude tremor leading up to the first magmatic explosion of the 2009 eruption at 6:38 March 23. Two hours of this sequence prior to explosion is displayed in Fig. 14A.

Table 2
Pros and cons of amplitude and frequency metrics.

Metric	Pros	Cons
Duration	Good metric for tracking event coda length.	Depends on STA/LTA trigger which behaves differently across different seismic signals.
Interevent time	High resolution perspective of temporal event distribution and variation through time.	Overwhelmed by large numbers of events making event distribution difficult to assess.
Event rate (hourly)	Easy to see event distribution over large time span.	Lacks fine patterns and trends in event spacing seen in interevent time.
Peak amplitude	Easy detection of station clipping. Not sensitive to changing noise levels.	Inability to resolve amplitude changes above clipping threshold. Sensitive to spurious peaks.
Peak-to-peak amplitude	Same as peak amplitude. Excellent detector of certain types of noise when used with peak amplitude.	Same as peak amplitude including clipping threshold limitation and sensitivity to spurious peaks.
RMS amplitude	Ability to resolve changes in amplitude above clipping threshold. Less sensitive to spurious peaks.	Low amplitude events affected greatly by noise levels.
Peak frequency	Less variation caused by SNR. Ability to track stable peaks through time.	Provides a narrow view of overall spectra, similar events can have large variation.
Center frequency	Useful for noise and low-SNR detection when combined with peak frequency.	Values of small to medium events skewed by SNR.
Frequency index	More holistic consideration of overall spectral content. Resolves variation and trends in event Spectra.	Values of small to medium events skewed by SNR. Values of large events skewed by clipping.

Multiplet analysis indicated that 2881 of the original 4900 events (approximately 59%) formed 28 individual families, a significantly higher count than any other swarm in the 2009 eruption sequence.

Table 3
A comparison of the maximum hourly event rate and total event count for single-station detection (SSD) and manually re-picked events are displayed for the 8 event swarms detected during the 2009 eruption. Swarms are listed chronologically with their respective start and end times. T1 and T2 swarms were no manually re-picked indicated by 'N/A'. The S3 swarm not manually re-picked, but was instead re-picked using a correlation detector indicated by a '*'.

			Max event rate		Event count	
Swarm	Start	End	SSD	Re-pick	SSD	Re-pick
T1	1/25/2009 10:47	1/25/2009 23:10	119	N/A	427	N/A
T2	1/30/2009 20:29	1/31/2009 00:20	108	N/A	201	N/A
S1	2/26/2009 3:00	2/27/2009 13:00	115	107	2095	1631
P1	3/20/2009 12:00	3/23/2009 6:34	163	209	5548	4900
P2	3/27/2009 0:00	3/27/2009 8:00	151	201	703	786
S2	3/29/2009 7:50	3/29/2009 9:00	183	273	203	293
P3	4/2/2009 19:00	4/4/2009 13:58	201	228	5437	6585
S3	5/2/2009 13:28	5/9/2009 23:49	269	662*	19807	37528*

These families formed a complex procession throughout the swarm, many of which exist concurrently suggesting numerous sources were simultaneously active. Fig. 9 shows the frequency index and peak frequency vs. time for the 14 largest families in the P1 swarm, the remaining 14 smallest families were withheld from this plot for the sake of ease of viewing. Individual events are color coded by family (numbered by order of first detection) with symbol size scaled to RMS amplitude. Of the 28 families, 8 exceeded an event count of 100 with one dominant family (family 04) containing 1023 events over the approximately 66 hour duration of the swarm. Correlation detection resulted in an increased 1516 events belonging to this dominant family, though the majority of the additional events identified using this technique had much lower amplitudes and SNR. The last detected event occurred 113 min prior to the explosion at 6:38.

Multiplet behavior during this swarm exhibits a division into two periods of activity, one prior to March 22, and one after (Fig. 9). The first period is dominated by three families with large amplitude and lower spectral content (families 02, 03, and 05), while the second

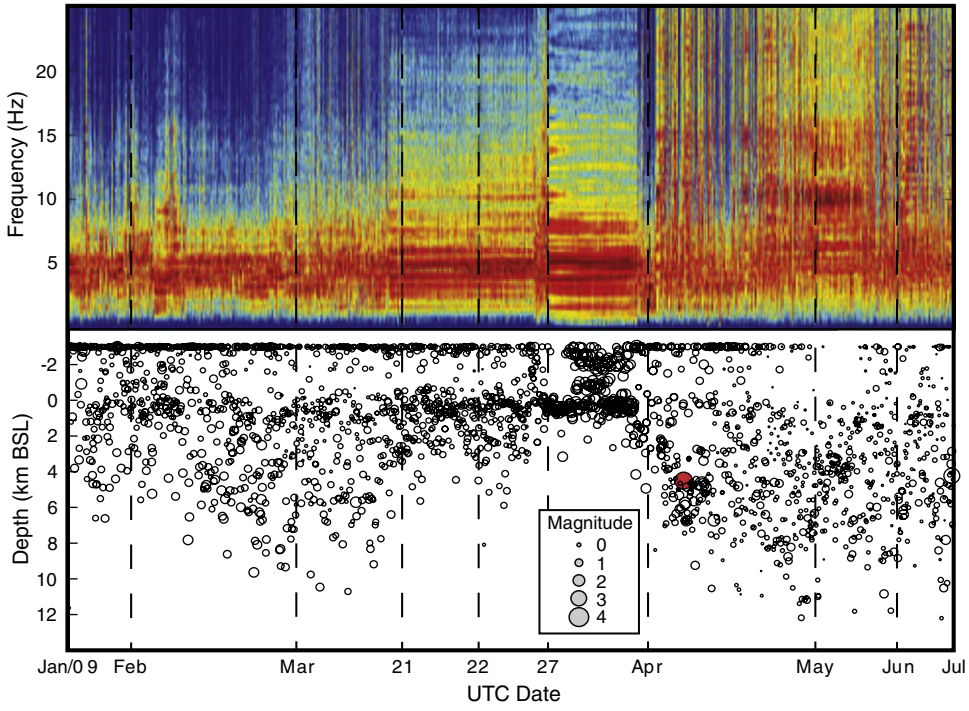

Fig. 6. Earthquake spectral amplitude (ESAM) calculated at station REF:EHZ (top), and depth and magnitude (bottom) of 2684 ARC earthquakes located at Redoubt between January 1 and June 30, 2009 (REF:EHZ). Event spacing is linear on the horizontal axis of the lower plot so that events are aligned with the ESAM plot. Symbol size in the lower plot is proportional to calculated magnitude. The largest magnitude earthquake ever located at Redoubt Volcano is highlighted in red on April 9 which had a computed magnitude of 3.5 and depth of 4.5 km BSL.

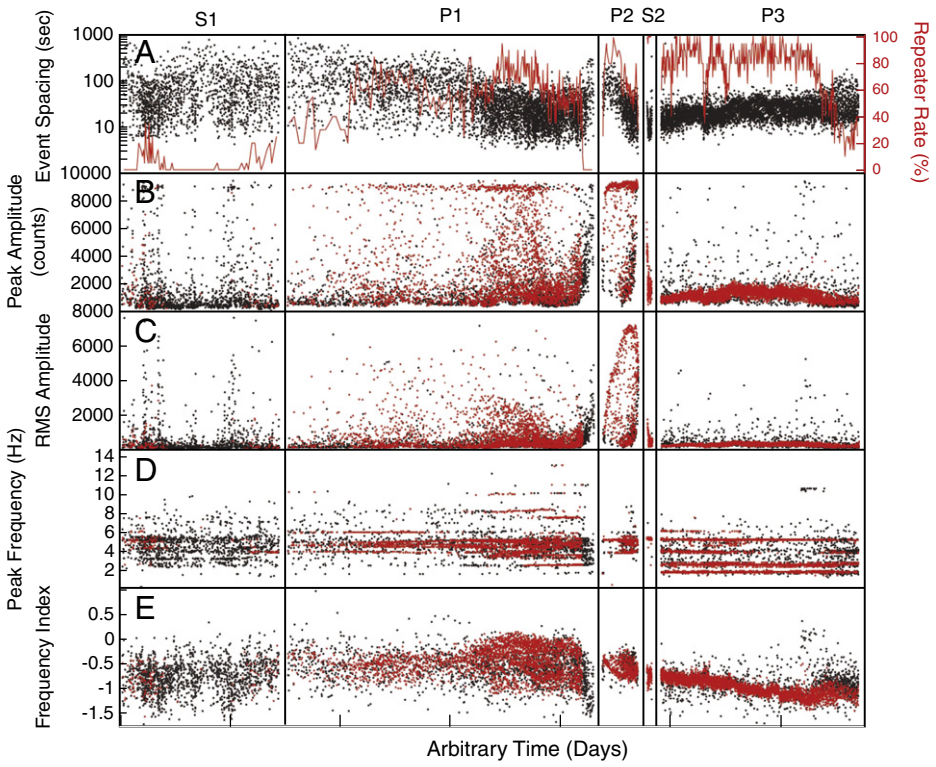

Fig. 7. Metrics of manually re-picked swarms (S1, P1, P2, S2, and P3) are plotted on the same arbitrary time scale separated by vertical spacers: (A) event spacing (black) and repeater rate as a percentage of overall event rate computed over bins of 20 events (red lines), (B) peak amplitude, (C) RMS amplitude, (D) peak frequency, and (E) frequency index. Red markers in plots B–E are events which formed multiplets, while black markers are non-multiplet events.

period is characterized by a more heterogeneous assortment of families with a wider range of amplitudes and spectral content (Fig. 9). Following March 22, multiplet rates reached several times to 80% and higher as seen in Fig. 7A. Detectable multiplets then disappear in the 2 h prior to the explosion. This may be a result of individual events being masked by high amplitude tremor during this period. Events from the dominant multiplet, family 04, spanned nearly the entire swarm becoming quicker in succession and higher in spectral content after March 22. These events had the highest FI values of any family and had distinct P and S phases suggesting the source may have involved some mode of brittle failure (Fig. 7D,E).

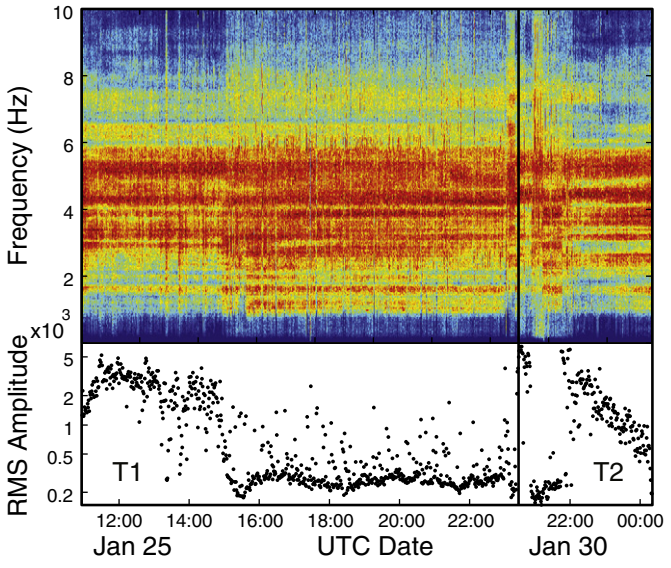

Fig. 8. Spectral amplitude and RMS amplitude were computed over 1 min sections of continuous REF:EHZ data during the T1 and T2 swarms (separated by vertical line).

The great variety of separate event families occurring throughout this swarm is a significant departure from the December 13–14, 1989 precursory swarm studied in depth by Stephens and Chouet (2001). During the 1989 swarm, one primary and two secondary LP event families were identified, all three of which shared similar spectral characteristics. The increased heterogeneity of the 2009 swarm suggests a greater number of active sources, different analysis techniques, different station configuration, or some combination of these factors. The range in spectral content including higher frequency families with more impulsive P and S phases also implies that some of the events recorded during the 2009 precursory swarm likely originated from brittle failure sources during the initial ascent of magma to the surface. A newly extruded lava dome was observed in satellite imagery at 20:00 March 22 (Diefenbach et al., 2013). The timing of this observation corresponds to a significant decrease in the rate and amplitude of the primary family, though the exact time of emergence of magma at the surface is unknown.

4.2.4. P2 swarm (March 27)

A strong precursory swarm began at 00:00 March 27 that lasted for approximately 8 h until a major explosion at 7:47. This swarm contained 703 events that were detected by SSD with a maximum hourly rate of 151 at 6:00. Manual detection increased the total number of events to 786 with a maximum hourly rate of 201 at this time. An estimated 300 events from this swarm clipped station REF. We place less focus on spectral characteristics of these events due to spectral distortion resulting from the high levels of clipping. Additionally, we manually picked 655 events from broadband station RDWB. This analysis was unique to this swarm and was undertaken to better understand the effects of station clipping on event metrics and also on the behavior of the correlation algorithm.

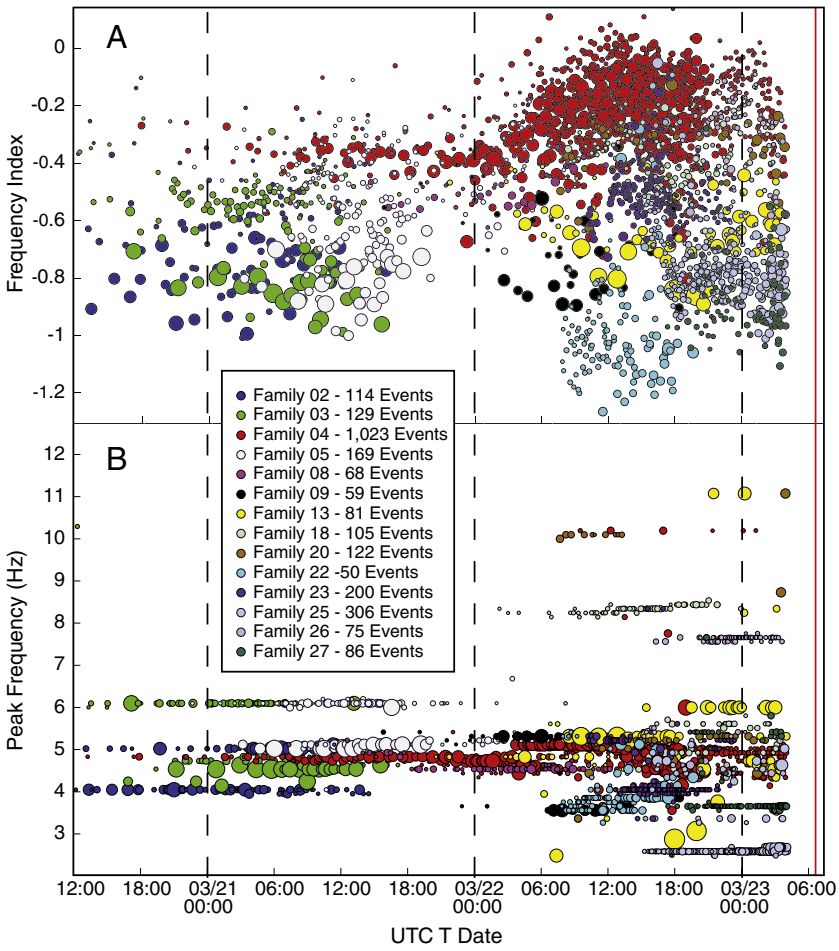

Fig. 9. (A) Frequency index and (B) peak frequency values are displayed for the largest 14 of the 28 families detected during the P1 swarm including all families with 50 events or more. Events in each family are identified by a unique marker color and marker size is proportional to event RMS amplitude. The time of the explosion at 6:38 3/23 is also marked by a vertical red line.

Correlation analysis revealed that 539 events (69%) of the manually picked events at REF formed 12 families of 10 or more events. The largest family contained 283 events (36%) with all remaining families containing 48 events or less. At station RDWB, 483 events grouped into only 6 families with the largest family containing 361 events (55%). Direct comparison of REF and RDWB relative arrival times revealed that 5 of the smaller families at REF were directly related to the dominant family. The splitting of the dominant family into multiple smaller families at REF is a phenomenon that depended more upon the correlation value and window length used and had less to do with instrument clipping. Correlation detection was also performed at station REF using a single event from the dominant multiplet occurring at 1:44:30. This detection resulted in 466 detected events overcoming the family 'splitting' observed using the previous technique. The last of these events occurred 8 min prior to the explosion at 7:47 (Fig. 14D).

The largest events of the swarm increased steadily from the onset of the swarm towards a peak about one hour before the explosion. Though peak amplitude values at REF were severely clipped, RMS amplitude values continued to register this increase (Fig. 7B,C). These larger events form an upper envelope to the peak amplitude data which appeared distinct from a concentration of lower amplitude events. REF and RDWB independently detected a change in event waveforms between 7:10 and 7:40 which are identified as secondary multiplets, though these events still correlate well with the dominant multiplet. These events merge into continuous tremor roughly 8 min before the explosion generating a frequency gliding phenomenon studied by Hotovec et al. (2013).

4.2.5. S2 swarm (March 29)

A short 70 minute long swarm of repeating events began abruptly at 7:52:53 on March 29 after a lull in seismic activity following an explosion at 3:23 of the same day. A total count of 293 events were manually selected from REF:EHZ during this swarm, an increase of 20 events from the 273 detected from SSD. The largest events of the swarm occurred first as measured both by peak amplitude and RMS amplitude. A cluster of 33 events from early in the swarm is distinct as having greater amplitude, event spacing, and FI values as seen in Fig. 10. Event amplitudes drop off after this initial cluster and events began to occur closer in time. A correlation exists between event spacing and amplitude throughout portions of this swarm. In general, larger events were preceded by larger gaps, which held even while larger and smaller amplitude events were occurring simultaneously. Event spacing after 8:10 appears to cluster into two distinct time-varying bands which converge and then split again, continuing until 8:36. This pattern is also discernible in the event amplitude data over the same time periods. Fig. 10D shows 2.5 min of REF:EHZ waveform data beginning at 8:17:00 and containing 18 events that alternate between larger and smaller amplitude. The lower band seen in the event spacing plot is the spacing from larger to smaller events, while the upper band is spacing from smaller to larger events.

Of the 293 events manually selected on REF, 290 were members of the same multiplet. These waveforms correlate highly throughout the swarm with little waveform evolution visible. Event spectra were highly consistent throughout the swarm. FI values had the smallest range of any swarm, over 97% of which fell between −0.6 and −1 (Figs. 7, 10).

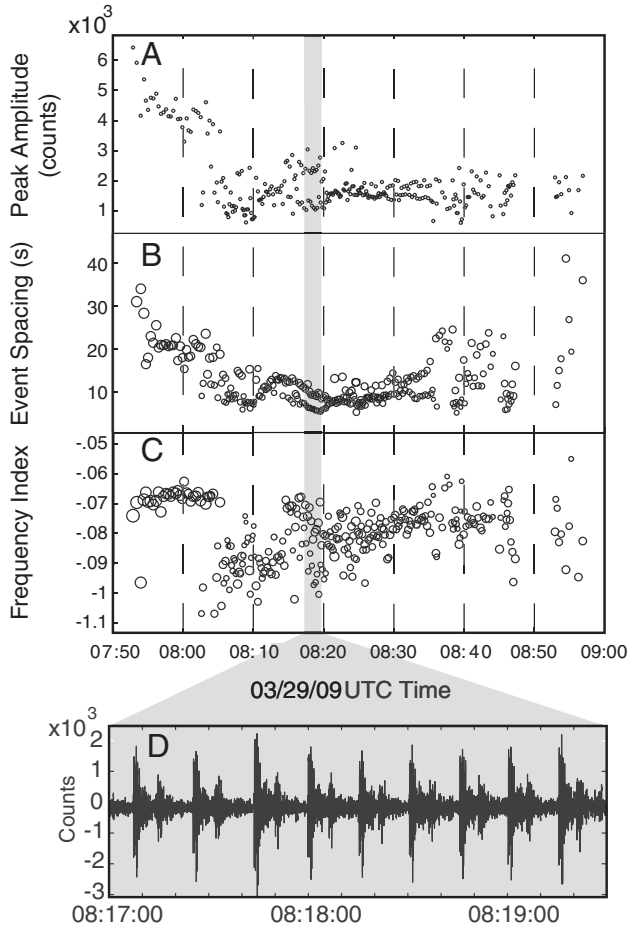

Fig. 10. (A) Peak amplitude, (B) event spacing, and (C) frequency index from the 290 events of swarm S2 which formed one single family. Highlighted in gray are the 18 events displayed in (D) which alternate between larger and smaller amplitude illustrating a pattern of positive correlation between event amplitude and interevent time to previous event. This trend persists through parts of the S2 swarm generating a bifurcation in the interevent time data.

4.2.6. P3 swarm (April 2–4)

The final precursory swarm of 2009 began abruptly at 19:00 on April 2 and lasted 43 h before culminating in the largest magmatic explosion of the 2009 eruption (Power et al., 2013). SSD detected 5437 events while manual selection increased the result to 6585 events. The first 14 h of the swarm exhibited sustained high event rates with four peaks above 200 events per hour with a maximum rate of 228 events per hour during the second hour of the swarm. Event rate dropped in the last 30 h below 150 events per hour, finally dropping below 100 events per hour in the final hour before explosion (Figs. 3, 7). Peak amplitudes were generally low throughout the swarm with less than 4% of events rising above 2000 counts at REF. Larger events are distributed throughout the swarm with one notable cluster of large high frequency events that occurred around 2:30 on April 4. The five highest amplitude events of the swarm occurred during this cluster within a period just over 1 h (Fig. 7).

Of the initial 6585 manually selected events, 4962 (75%) formed one dominant family with three more families containing only 45, 15, and 18 events. The size of the dominant multiplet jumped to 6273 events using correlation detection with an initial reference event from 12:11:07 April 3. Dominant family waveforms were low in amplitude from the onset of the swarm. FI values tracked an overall spectral trend moving from higher to lower frequency (Fig. 7), and dominant family waveforms exhibited a loss of higher frequency energy in the first few seconds of each waveform following the P arrival. FI values were lowest before 3:00 on April 4, consistent with the occurrence of the previously mentioned cluster of high frequency events. Following the cluster, event rate steadily dropped as events became smaller in amplitude. FI values increased and also assumed a wider range from the previously tightly clustered trend, likely caused by the drop in event SNR. This period contained all three smaller families which were similar to the dominant family in both amplitude and spectral content. Non-family events had a broad range of amplitudes and spectral content throughout the swarm which contained many of the highest and lowest frequency events, as well as all large amplitude events seen in Fig. 7.

Though the high frequency cluster represents a small percentage of overall seismicity, we place some importance on its presence and the role it seemed to have played as a 'tipping point' leading into the final hours before dome failure and explosion. These events formed a multiplet which continues after explosion 19 though most of April and is examined in detail in Section 4.3. The presence of these high frequency events, change in spectral behavior, and decline of family waveforms may have been good indicators of a shift to potentially explosive conditions within the shallow magmatic system. Similar seismic patterns preceded many explosions in the 1989–90 eruption of Redoubt (Stephens et al., 1994).

4.2.7. S3 swarm (May 2–9)

A swarm of low frequency, low amplitude repetitive events began on May 2 and lasted until May 9 during a period of dome growth. The number of events from this swarm was over double that of all other swarms during the 2009 eruption combined. Attempting to manually pick these events would have been overwhelming, yet the repetitive nature of these events allowed for robust detection of events using correlation detection. A single reference waveform from 02:58:59 March 6 was used resulting in 37,528 events, the great majority of which occurred between May 3 and May 8. The detector exhibited certain strengths over STA/LTA detection, the first of which included the ability to detect low SNR events that occurred near the beginning and end of the swarm as the seismic process faded into background noise. Secondly, this method was able to resolve individual events even as interevent time approached and dropped below the 6 second detection window. Metrics for the S3 swarm are shown in Fig. 11.

Event rate in the S3 swarm increased rapidly beginning on May 3 then waxed and waned for three days reaching above 300 events per hour several times. Interevent spacing of these events assumed an interesting distribution with division into distinct bands occurring May 3–4 and again on May 8 (Fig. 11B). This phenomenon could be a direct result of low SNR events being missed by the detector.

On May 6, a major shift in behavior took place in which event rate dropped rapidly, then jumped up to an unprecedented rate above 500 events per hour, peaking at 662 events per hour early on May 7. This shift is clearly seen as a scattered spike occurring above a dramatic and immediate drop in event spacing (Fig. 11B). This change in event rate coincided with a sequence of large rockfalls that occurred on the growing lava dome and were captured by the web camera operated by AVO 12 km north of the volcano. A helicorder plot from REF and the webcam images displayed in Fig. 12 were taken during the rockfall sequence. The times of the twelve images in this figure are marked with stars on the helicorder plot. The rockfall signals are concurrent with a disruption of the slower and steadier procession of repeating events (colored red) leading to an unstable procession in which clusters of tightly spaced repeating events are separated by longer gaps. The gaps between these tightly spaced event clusters appears to be nearly random, though a steady overall decline in gap size does occur which lasts well into May 7 seen in Fig. 11. These observation suggest a direct linkage between the conditions on the surface of the lava dome and the source of the repeating seismic events (Fig. 12). A large decline in event rate occurred later on May 7 with another minor peak on May 8 before events fade out. Slow but steady waveform evolution existed throughout this swarm including a dampening of the more energetic onset immediately following the P arrival that is similar to waveform evolution during the P3 swarm.

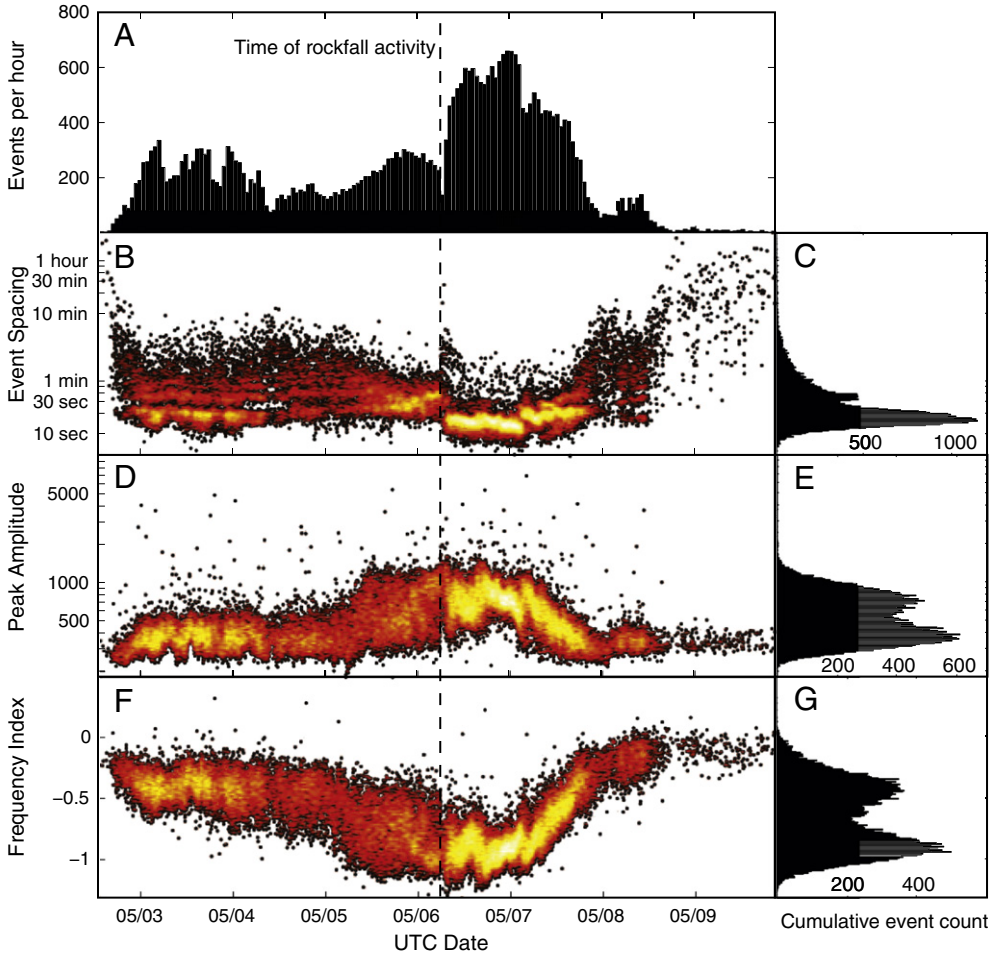

Fig. 11. Metrics of 37,528 events in the dominant S3 multiplet resulting from correlation detection including (A) hourly event rate, (B) Event spacing, (D) Peak amplitude, and (F) frequency index. Plots B, D, and F have been overlaid with an image which maps relative density of markers in the scatter plot to heat values. This gives a visual representation of marker density beyond the point at which these plots would otherwise be saturated (solid black). Plots C, E, and G show the cumulative distribution of metric values plotted in B, D, and F.

4.3. SSD multiplets

Multiplet detection was iteratively performed over all SSD events resulting in 238 initial event families. Because multiplet detection had been fully automated, waveforms from each family were manually inspected for legitimacy. A total of 92 families were removed after inspection on account of having low SNR or very short-lived or impulsive waveforms. The remaining 146 event families are examined in the remainder of this section. One notable period of family removal occurred during the S3 swarm. A total of 28 small event families were eliminated after it was discovered that the combined high event rate and low SNR of the events in these families were preventing them from connecting to the dominant S3 family. Many of these events were able to form smaller multiplets, often resulting from events with very similar event spacing and overlap with adjacent events. Correlation detection performed remarkably well at identifying these events as one single multiplet, thus it was unnecessary to further expand the completeness of the dominant family resulting from SSD.

The size of resulting multiplets ranged between 13,921 (S3 multiplet) and 10 (the required minimum). 84 of these multiplets began during the precursory phase (28 of these during the P1 swarm), 15 during the explosive phase, and 47 during the continuous phase. Families did not span multiple phases with only one exception: the high frequency cluster towards the end of the P3 swarm on April 4 continues after explosion 19 until April 22. Fig. 13 displays repeater rate, FI, and RMS amplitude of the 146 families detected throughout the study period as well as during the explosive phase. Dominant event families which preceded seven explosions are examined in greater detail in 4.4.

Multiplet seismicity behaved very differently throughout portions of the eruption as displayed by median FI and median RMS amplitude values seen in Fig. 13(B). A rapid succession of new multiplets occurred during the T1 and T2 swarms in late January as well as the S1 swarm in late February which divides the precursory phase into distinctly separate periods. Late January multiplets, for instance, had a larger spread of frequency index and amplitude values indicating a greater diversity is repeating processes than those that had occurred leading up to this period. Likewise, the continuous phase is divided by the S3 swarm with distinctly separate characteristics before and after.

The presence of high frequency multiplets is a unique feature of the continuous phase. Five high frequency or VT multiplets were identified during this period which had mean peak frequency values above 9 Hz in addition to mean frequency index values above 0.2. These five multiplets contained 22, 19, 26, 88, and 14 events respectively. These families corresponded to 10, 12, 12, 45, and 8 ARC locations representing a location rate above 50% which is significant considering that approximately 2% of SSD events from this study had ARC locations. In Fig. 15(A), depth and magnitude of the located events from each family are plotted as well as a dashed line indicating the median depth of each family. One waveform from each VT family is displayed in Fig. 15(B). The deepest two families occur throughout the same period in late April and early May leading into the S3 swarm. The deepest family locates consistently at a depth 7 km below sea level putting it at comparable depth to the

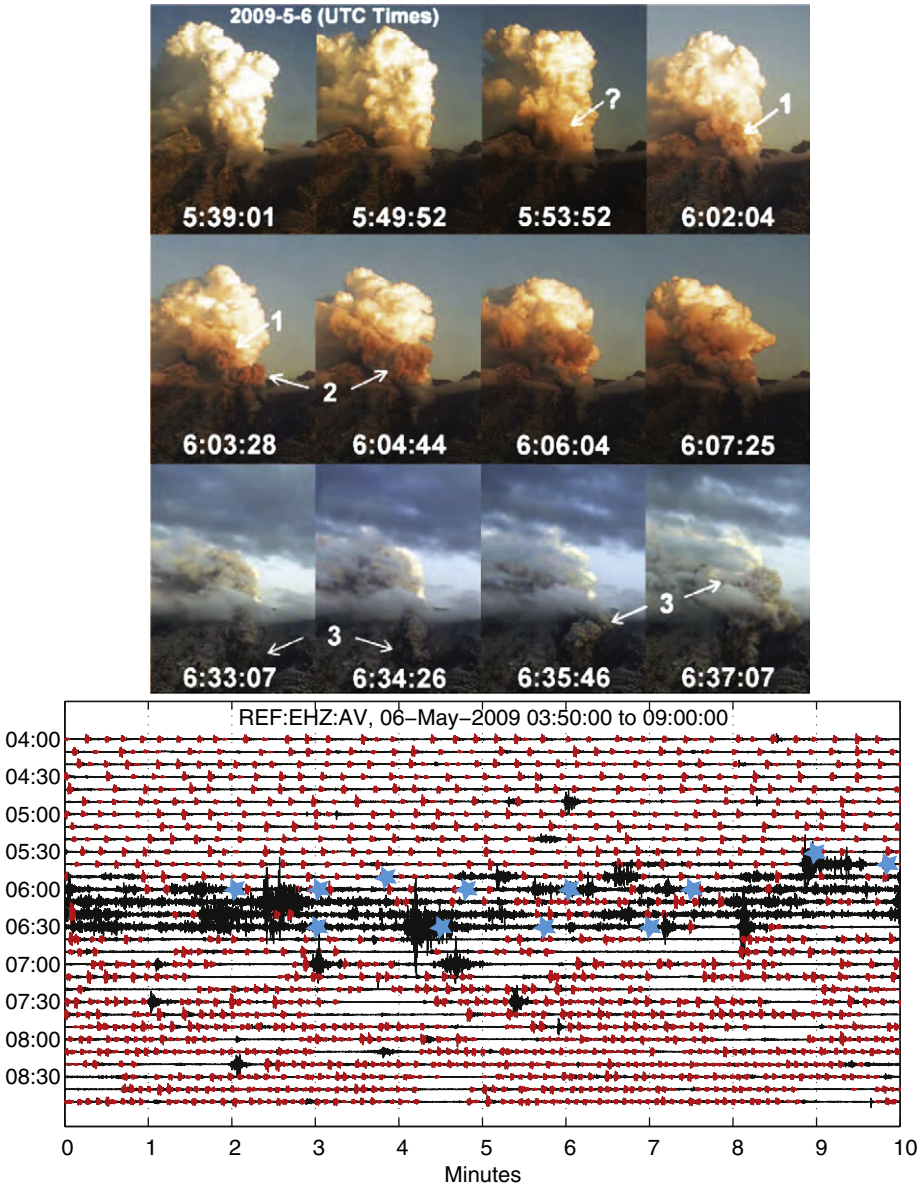

Fig. 12. (Top) 12 frames from a Redoubt webcam captured at least three dark plumes during a period of rockfall on May 6 which is believed to be generated by partial dome failure. (Bottom) This seismic sequence is displayed as a helicorder plot with overlayed blue markers indicating when each image was taken. Events from the dominant S3 multiplet are colored red. A clear shift in the procession of these events can be seen between the top and bottom of the helicorder plot.

inferred magma storage region at 6–10 km below sea level (Power et al., 1994, 2013; Browne and Gardner, 2006). The remaining families locate in a range approximately 1–3 km below sea level.

4.4. Precursory multiplets

Three precursory swarms were identified from SSD event rate, yet SSD multiplet detection revealed a total of seven explosions were preceded by multiplets (Fig. 13C,D) including explosions 1,3,6,9,12,18, and 19. The dominant multiplet occurring prior to each of these explosions was detected using correlation detection which resulted in substantial increases in the number of events detected. Fig. 14(A-G) shows waveform data corresponding to 2 h before, and half an hour following the onset of each of these explosions with individual multiplet events highlighted in red. The size of precursory multiplets ranged from 21 events before explosion 3 to 6,273 events before explosion 19. Precursory multiplets behaved somewhat differently with respect to amplitude and event spacing. Events occurring prior to explosions 6, 9, and 18 exhibited dramatic increases in event rate in the final hour leading up to explosion (Fig. 14C,D,F). By contrast, those prior to explosions 1 and 19 (P1 and P3 swarms) experienced a trend towards lower and more scattered event rates towards the end of each multiplet (Fig. 14A,G). High amplitude tremor in the 2 h prior to explosion 1 makes it difficult to assess multiplet activity, though it is still clear that events from the dominant multiplet had dropped significantly in amplitude and rate prior to the onset of this tremor. Multiplet events prior to explosions 1, 9, 18, and 19 displayed a drop in amplitude near the end of each multiplet while events prior to explosions 6 and 12 displayed increases in amplitude preceding explosions. Multiplet event clusters preceded over 50% of ash producing explosions at Augustine in 2006 (Buurman and West, 2010). Multiplet clusters at Redoubt in 2009 only preceded 37% of ash producing explosions, though we note that many of the explosions occurred close together in time. Explosions 1–5 for instance occurred within a six hour span while explosions 12–18 occurred

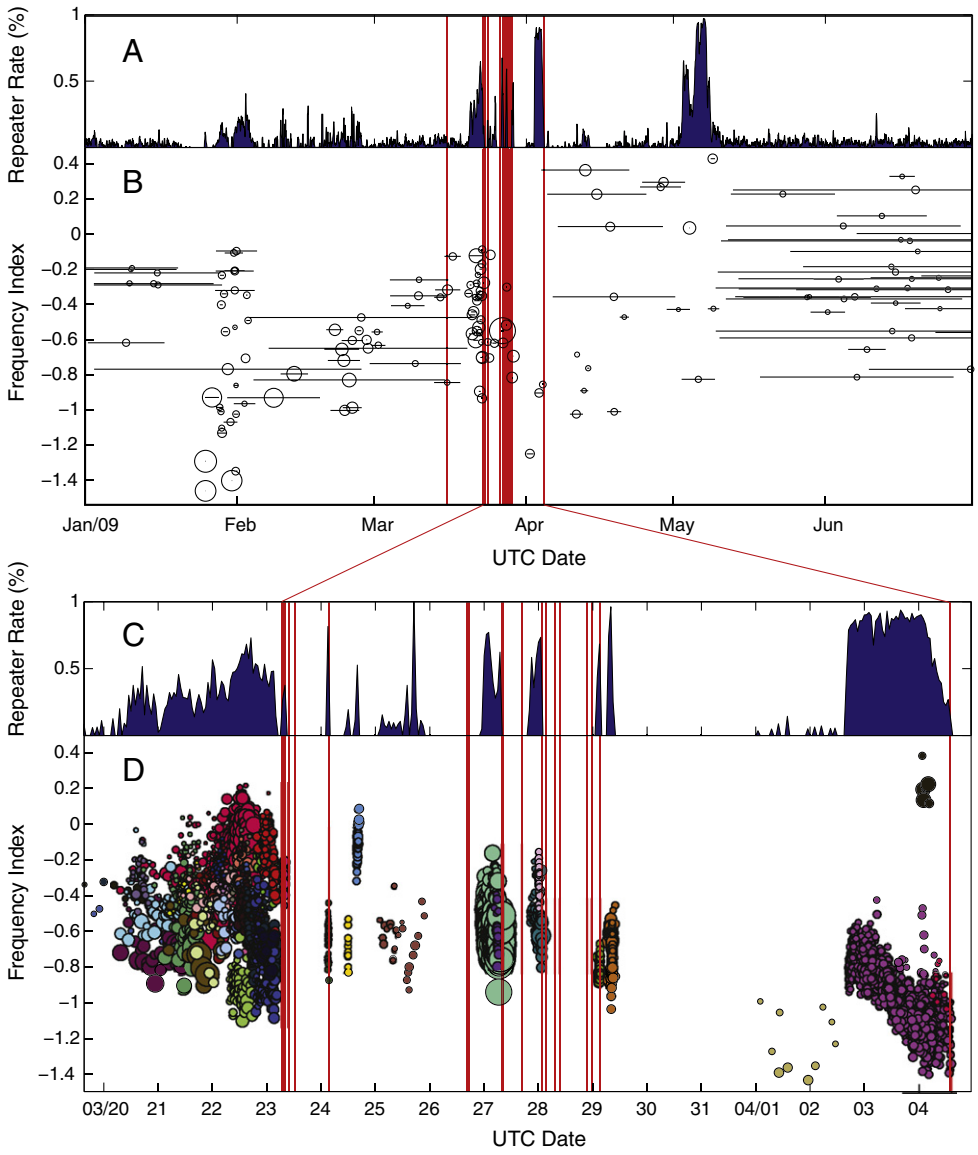

Fig. 13. (A) SSD repeater rate measures the percentage of multiplet events to overall SSD events. (B) Median frequency index vs. time of 146 families resulting from SSD multiplet detection. The size of each circular marker is proportional to the median RMS amplitude value of all events in the family. A horizontal line through each marker indicates the span of time that each family existed reaching from the start time of the first to the last event. (C) Repeater rate from P1 to P3 swarm. (D) frequency index vs. time from P1 to P3 swarm with marker color indicating different families and marker size proportional to event RMS amplitude. Vertical red lines in all plots indicate the time of explosions.

in just over 24 h. Strong tremor before at least four explosions made multiplet detection impossible. Of the 22 significant tephra-producing explosions at Redoubt in 1989–90, 11 were preceded by LP swarms lasting over an hour (Stephens et al., 1994). Though waveform similarity was high during some of these swarms, we lack a complete record of similarity during all detected swarms. The relationship between multiplet activity and explosive conditions is an important one that should be considered in future monitoring efforts.

4.5. Limitations and future research

Single station detection proved successful in identification and characterization of a much more complete set of seismic events throughout the 2009 eruption than the events selected for hypocenter and magnitude calculation (Power et al., 2013). This single station technique was not however without significant limitations including an inherent and pervasive single station bias. Most events were not verified or characterized at other stations making proximity of seismic sources to station REF an uncontrolled variable affecting both amplitude and spectra of the resulting observations. The short period instrument used in this study had a natural frequency of 2 Hz with a response curve that was attenuated at lower frequencies. Additionally, spectra from numerous events observed at other stations showed that spectral peaks were highly variable between stations arising largely from site and path effects. This led to a general de-emphasis in this study of the significance of individual spectral peaks with more of a focus applied to general spectral trends including the ratio of higher to lower frequencies used in the frequency index metric. Future improvements upon the current single station approach should include detections from multiple stations as well as an automated procedure for identifying spectral peaks that are consistent across multiple stations.

We believe that single station event detection and classification could prove to be indispensable tools for monitoring an eruption, especially where a limited number of seismic stations are operational. All data processing methods used in this study could in theory be adapted to a database system operating in near-real-time. To prove useful during

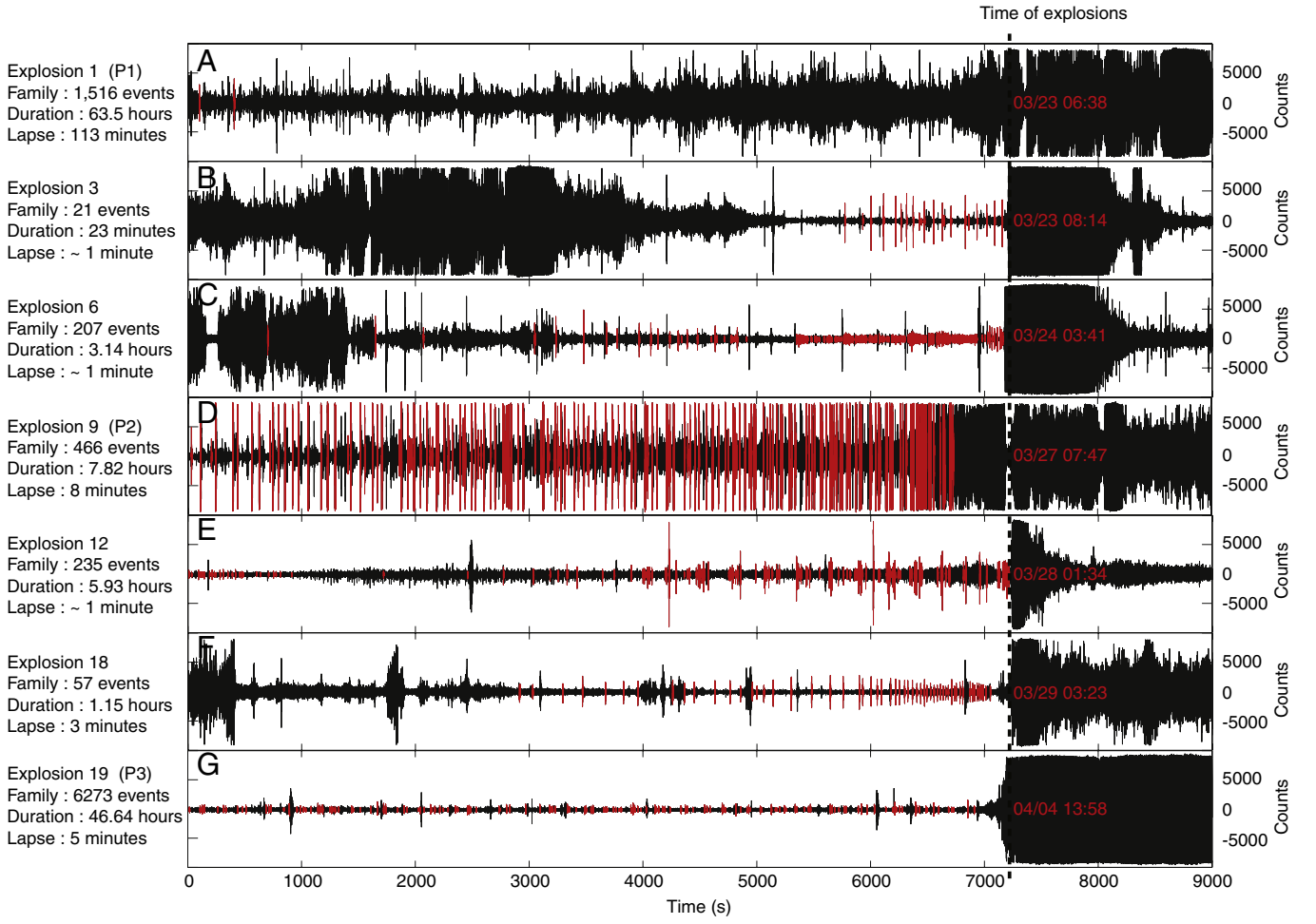

Fig. 14. Waveform data from REF is displayed for the 7 explosions that were preceded by multiplet clusters including (A) explosion 1 at 06:36 3/23, (B) explosion 3 at 8:14 3/23, (C) explosion 6 at 3:41 3/24, (D) explosion 9 at 7:47 3/27, (E) explosion 12 at 1:34 3/28, (F) explosion 18 at 3:23 3/29, and (G) explosion 19 at 13:58 4/4. Two hours of data are displayed prior to, and half an hour following the onset of each explosion. Events from each dominant family were detected using correlation detection and are highlighted in red. Displayed to the left of each seismogram is information detailing the number of events detected in each cluster, the duration of the cluster, and the lapse between the start of the last event and the onset of the respective explosion.

an eruption crisis, such a system would need to be largely automated with a minimal requirement for user input or manipulation. Manual noise removal and manual event detection during swarms were two time-intensive procedures performed in this study that could not be afforded during an eruption crisis. In this study we have also successfully tested automated procedures for removing noise using event metric thresholds listed in B. Additionally, the success of single-station detection combined with correlation detection have worked sufficiently to make manual event review and selection unnecessary.

Previous studies by DeShon et al. (2007, 2010) have used event similarity among events within the analyst reviewed catalog to more accurately determine phase arrival times from aligned waveform stacks. Because the catalog only represents a small percentage of the total seismic events occurring during an eruption, we assume that a great majority of multiplet events are also being omitted. In this study, we detected nearly 150 different event families from the suite of single station detection events. We also demonstrated the robust ability of an evolving correlation detector to further expand the number of detectable multiplet events. Stacking waveforms to increase SNR from this wealth of multiplet events could greatly increase the number of events which could be located. Automated multiplet detection and waveform alignment would also allow analysts to quickly pick arrivals from waveform stacks thereby reducing latency. An increase of event location information could prove very useful in forecasting volcanic unrest. This is especially true with multiplet events considering their relation to explosions.

5. Summary and conclusions

In this study we detected and characterized seismic events at Redoubt Volcano between January 1 and June 30, 2009 on short-period edifice station REF. Events were detected with an STA/LTA algorithm, with a manual picking procedure, and with a correlation detection algorithm. Detected events were characterized using nine metrics that included event duration, inter-event time, event rate, peak amplitude, peak-to-peak amplitude, RMS amplitude, peak frequency, center frequency, and frequency index. The single station approach was very successful at detecting and characterizing small seismic events within the 2009 eruptive sequence that were not large enough for standard hypocenter and magnitude determination.

Our analysis indicates that the 2009 eruption of Redoubt produced a wide variety of seismic activity including earthquakes spanning a large range of amplitudes, durations, and spectral content. Many of these events fit descriptions of LP, hybrid, and VT event types that have been previously studied at Redoubt (Lahr et al., 1994), though no direct link to these event types is established in this study. General volcanic behavior includes two months of precursory tremor, 19

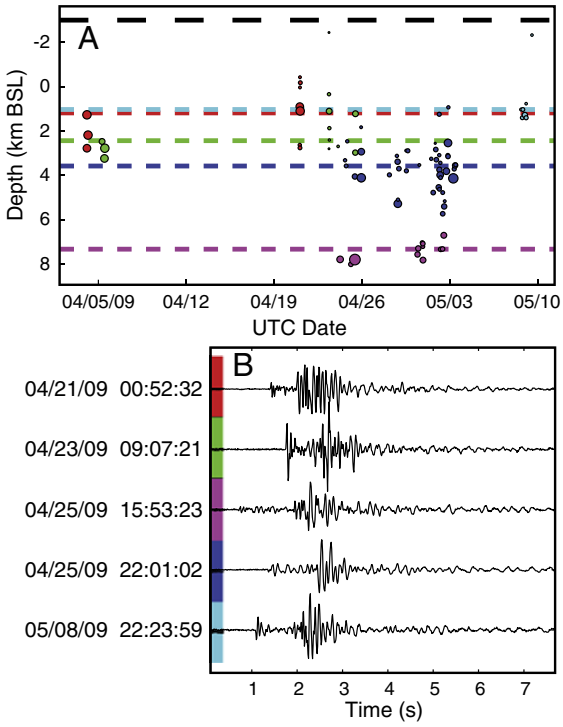

Fig. 15. (A) ARC depth and magnitude vs. time of five identified VT multiplets. Dashed color lines correspond to the median depth of that particular family. The black dashed line at 3 km ASL indicates the crater floor and top of the velocity model, (B) example waveforms are plotted from each VT multiplet.

explosions spanning a two week period, event swarms, a complex distribution of event families or multiplets, and a continuous phase of lava effusion that was marked by increased VT earthquakes and large low frequency events. A summary of our analysis and observations includes:

(1) Nine metrics were used in varying capacities to characterize the amplitude, spectra, length, and temporal distribution of events and detect noise events. Pros and cons of each metric are summarized in Table 2. The combination of SSD, event metric analysis, and multiplet analysis proved to be a robust approach to tracking the complex procession of seismic signals associated with the 2009 eruption. These techniques could prove useful in a near real-time monitoring capacity with the potential to alert staff to more subtle changes in seismic behavior during future periods of unrest.

(2) This analysis revealed eight swarms with event rates that exceeded 100 events per hour. January 25 (T1) and 30–31 (T2) swarms are associated with high amplitude spasmodic tremor. Swarms on March 20–23 (P1), March 27 (P2), and April 2–4 (P3) immediately preceded magmatic explosions while February 26–27 (S1), March 29 (S2), and May 2–9 (S3) were not terminated by explosions. Swarms that were not terminated by explosions were unique to the 2009 eruption, since all swarms identified during the 1989–90 eruption ended with an explosion (Stephens et al., 1994).

(3) The initial precursory swarm (P1) in 2009 on March 20–23 contained 28 different families and events exhibited a broad range of amplitudes and spectral content. Many of the events from this swarm have broad spectra and are believed to involve brittle failure sources. Swarms on March 27 (P2), March 29 (S2), April 2–4 (P3), and May 2–9 (S3) were more homogeneous, all of which were composed primarily of one dominant family. The largest single family spanned May 2–9 (S3) and contained 37,538 events.

(4) A significant decrease in event rates of the dominant families occurred prior to March 23 and April 4 explosions.

(5) February 26–27 swarm had the five highest event amplitudes of any swarm, March 27 swarm had highest average amplitudes, and April 2–4 swarm had the lowest average amplitudes.

(6) January 25 (T1) and 30–31 (T2) swarms had the lowest average spectral content, while March 20–23 (P1) swarm had the highest.

(7) A sudden shift in the procession of repeating events on May 6 immediately followed rockfall from the growing dome, suggesting a link between surface activity and the earthquake source.

(8) A total of 146 event families were detected throughout the eruption. Families covered a large range of waveform character including FI values from −1.5 to 0.4 and RMS amplitude values from 100 to 7,232.

(9) Of the 19 explosions during the 2009 eruption sequence, 7 were preceded by clusters of one of more event families including explosions at 06:38 3/23 (P1), 08:14 3/23, 3:41 3/24, 7:47 3/27 (P2), 1:34 3/28, 3:23 3/29, and 13:58 4/4 (P3).

(10) A heightened level of high frequency events persisted throughout the continuous phase of the eruption. Many of these high frequency events formed at least 5 different families. The appearance of these 'VT families' occurred on April 4 h prior to the final magmatic explosion and continued until early May.

Appendix A. STA/LTA detection parameters

A complete description of the Short-Term Average, Long-Term Average (STA/LTA) algorithm used in single-station detection is provided in Table A.4. This algorithm was performed continuously over day-long sections of REF:EHZ waveform data. The algorithm used a 'frozen' post-trigger LTA behavior meaning that the Long-Term Average window would retain its value after the STA/LTA ratio exceeded the threshold t_{on}. The Short-Term Average window continues to update until the STA/LTA ratio drops back below the threshold t_{off}. This behaves differently that a 'continuous' LTA window which updates continuously regardless of the state of the trigger. In general, the frozen window returns much longer durations for large events, but is

Table A.4
STA/LTA parameters used in single-station event detection.

Variable	Value	Description
L_{STA}	1 s	Length of short-term window
L_{LTA}	7 s	Length of long-term window
t_{on}	2.0	Trigger-on threshold
t_{off}	1.6	Trigger-off threshold
dur_{min}	1.6 s	Minimum event duration
dur_{skip}	3 s	Skip ahead after end of event

Table B.5
Extreme metric values used for SSD noise removal including RMS amplitude (RMSA), peak frequency (PF), center frequency (CF), peak-to-peak amplitude (P2P), duration (DUR), and frequency index (FI).

Metric values removed	Count
RMSA<100	3432
PF<1 Hz and>16 Hz	4656
CF/PF > 10	1115
P2P/RMSA>17 or P2P/RMSA>13 if DUR<6) or P2P/RMSA>11 if DUR < 3)	669
(FI>0.6) or (FI>0.4 if DUR<4) or (FI>0.2 if DUR<3)	1016
(Combined total)	9881

also consequently unable in some special case to get out of the trigger state. This was largely avoided in this study through the manual removal of noise.

Appendix B. SSD event noise detection

SSD Events associated with noise and very low SNR were stripped from the overall event set. Table B.5 lists the metric threshold values used as well as the number of events removed. The total events removed from the SSD set is less than the sum of each of the counts presented as a result of some overlap between sets of noise events.

References

Allen, R.V., 1978. Automatic earthquake recognition and timing from single traces. Bulletin of the Seismological Society of America 68 (5), 1521–1532.

Browne, B.L., Gardner, J.E., 2006. The influence of magma ascent path on texture, mineralogy, and formation of hornblende reaction rims. Earth and Planetary Science Letters 246, 161–176.

Bull, K., Buurman, H., 2013. An overview of the 2009 eruption of Redoubt Volcano, Alaska. Journal of Volcanology and Geothermal Research 259, 2–15.

Bull, K., Anderson, S.W., Diefenbach, A.K., Wessels, R.L., Henton, S.M., 2013. Emplacement of the final dome of the 2009 eruption of Redoubt Volcano, Alaska. Journal of Volcanology and Geothermal Research 259, 334–348.

Buurman, H., West, M., 2010. Seismic precursors to volcanic explosions during the 2006 eruption of Augustine Volcano. In: Power, J., Coombs, M., Freymueller, J. (Eds.), The 2006 eruption of Augustine Volcano. U.S. Geological Survey Professional Paper 1769, Alaska (U.S. Geological Survey Professional Paper 1769).

Buurman, H., West, M., 2013. The seismicity of the 2009 Redoubt eruption. Journal of Volcanology and Geothermal Research 259, 16–30.

Chouet, B., Page, R., Stephens, C., Lahr, J., Power, J., 1994. Precursory swarms of long-period events at Redoubt Volcano (1989–1990), Alaska: their origin and use as a forecasting tool. Journal of Volcanology and Geothermal Research 62, 95–135.

Coombs, M., Sisson, T., Bleick, H., Henton, S., Nye, C., Payne, A., Cameron, C., Larsen, J., Wallace, K., Bull, K., 2013. Andesites of the 2009 eruption of redoubt volcano, alaska. Journal of Volcanology and Geothermal Research 259, 349–372.

DeShon, H.R., Thurber, C.H., Rowe, C., 2007. High-precision earthquake location and three-dimensional P wave velocity at Redoubt Volcano, Alaska. Journal of Geophysical Research 112 (B07312).

DeShon, H.R., Thurber, C.H., Power, J.A., 2010. Earthquake waveform similarity and evolution at Augustine Volcano from 1993 to 2006. In: Power, J., Coombs, M., Freymueller, J. (Eds.), The 2006 eruption of Augustine Volcano. U.S. Geological Survey Professional Paper 1769, Alaska (U.S. Geological Survey Professional Paper 1769).

Diefenbach, A., Bull, K., Wessels, R., McGimsey, R., 2013. Photogrammetric monitoring of lava dome growth during the 2009 eruption of Redoubt Volcano. Journal of Volcanology and Geothermal Research 259, 308–316.

Dixon, J.P., Stihler, S.D., Power, J.A., Searcy, C., 2010. Catalog of Earthquake Hypocenters at Alaskan Volcanoes: January 1 Through December 31, 2009. U.S. Geological Survey Data Series 531.

Grapenthin, R., Freymueller, J.T., Cervelli, P., 2013. Geodetic observations during the 2009 eruption of Redoubt Volcano. Journal of Volcanology and Geothermal Research 259, 115–132.

Haney, M.M., Van Wilk, K., Preston, L.A., Aldridge, D.F., 2009. Observations and modeling of source effects in coda wave interferometry at Pavlof Volcano. Leading Edge (Tulsa, OK) 28, 554–560.

Hotovec, A.J., Prejean, S.G., Vidale, J.E., Gomberg, J., 2013. Strongly gliding harmonic tremor during the 2009 eruption of Redoubt Volcano. Journal of Volcanology and Geothermal Research 259, 89–99.

Lahr, J., 1999. HYPOELLIPSE: A computer program for determining local earthquake hypocentral parameters, magnitude, and first motion pattern. U.S. Geological Survey Open-File Report, pp. 99–123.

Lahr, J., Chouet, B., Stephens, C., Power, J., Page, R., 1994. Earthquake classification, location, and error analysis in a volcanic environment: implications for the magmatic system of the 1989–1990 eruptions at Redoubt Volcano, Alaska. Journal of Volcanology and Geothermal Research 62, 137–151.

Latter, J., 1979. Volcanological observations at tongariro national park, 2 types and classification of volcanic earthquakes, 1976–1978, Volume 2. Geophysics Division, Department of Scientific and Industrial Research, pp. 1–60 (150).

Lopez, T., Carn, S., Werner, C., Kelly, P., Doukas, M., Fee, D., Webley, P.W., Cahill, C., Schneider, D., 2013. Evaluation of Redoubt Volcano's sulfur dioxide emissions by the Ozone Monitoring Instrument. Journal of Volcanology and Geothermal Research 259, 290–307.

Miller, T., Chouet, B., 1994. The 1989–1990 eruptions of Redoubt Volcano: an introduction. Journal of Volcanology and Geothermal Research 62, 1–10.

Minakami, T., 1960. Fundamental research for predicting volcanic eruptions. 1. Earthquakes and crustal deformations originating from volcanic activities. Bulletin of the Earthquake Research Institute-University of Tokyo 38, 497–544.

Moran, S.C., Malone, S.D., Qamar, A.I., Thelen, W.A., Wright, A.K., Caplan-Auerbach, J., 2008. Seismicity Associated with Renewed Dome Building at Mount St. Helens, 2004–2005. In: Sherrod, D.R., Scott, W.E., Stauffer, P.H. (Eds.), A Volcano Rekindled: the Renewed Eruption of Mount St. Helens, 2004–2006. U.S. Geological Survey Professional Paper 1750, pp. 27–60 (U.S. Geological Survey Professional Paper 1750, Ch. 2).

Power, J., Lahr, J., Page, R., Chouet, B., Stephens, C., Harlow, D.H., Murray, T.L., Davies, J.N., 1994. Seismic evolution of the 1989–1990 eruption sequence of Redoubt Volcano, Alaska. Journal of Volcanology and Geothermal Research 62, 69–94.

Power, J., Stihler, S., Chouet, B., Haney, M.M., Ketner, D.M., 2013. Seismic observations of Redoubt Volcano, Alaska —1989–2010 and a conceptual model of the redoubt magmatic system. Journal of Volcanology and Geothermal Research 259, 31–44.

Qamar, A.I., Malone, S.D., Moran, S.C., Steele, W.P., Thelen, W.A., 2008. Near-real-time Information Products for Mount St. Helens–Tracking the Ongoing Eruption. In: Sherrod, D.R., Scott, W.E., Stauffer, P.H. (Eds.), A Volcano Rekindled: the Renewed Eruption of Mount St. Helens, 2004–2006. U.S. Geological Survey Professional Paper 1750, pp. 61–70 (Ch. 3).

Robinson, M., 1992. Xpick user's manual v4.2, p. 119.

Schaefer, J., 2012. The 2009 eruption of Redoubt Volcano, Alaska. Division of Geological & Gephysical Surveys Report of Investigations 2011–5, pp. 1–45.

Stephens, C., Chouet, B., 2001. Evolution of the December 14, 1989 precursory long-period event swarm at Redoubt Volcano, Alaska. Journal of Volcanology and Geothermal Research 109, 133–148.

Stephens, C., Chouet, B., Page, R., Lahr, J., Power, J., 1994. Seismological aspects of the 1989–1990 eruption at Redoubt Volcano, Alaska: the SSAM perspective. Journal of Volcanology and Geothermal Research 62, 153–182.